The epidermal circadian clock integrates and subverts brain signals to guarantee skin homeostasis

Thomas Mortimer[1*], Valentina M. Zinna[1], Muge Atalay[1], Carmelo Laudanna[1], Oleg Deryagin[2], Guillem Posas[1], Jacob G. Smith[2,3], Elisa García-Lara[1], Mireia Vaca-Dempere[2], Leonardo Vinícius Monteiro de Assis[4], Isabel Heyde[4], Kevin B. Koronowski[5], Paul Petrus[3,6], Carolina M. Greco[7,8], Stephen Forrow[1], Henrik Oster[4], Paolo Sassone-Corsi[3], Patrick-Simon Welz[9*], Pura Muñoz-Cánoves[2,10,11*], Salvador Aznar Benitah[1,10,12*]

1. Institute for Research in Biomedicine (IRB Barcelona), The Barcelona Institute of Science and Technology (BIST), 08028, Barcelona, Spain.

2. Universitat Pompeu Fabra (UPF), Department of Medicine and Life Sciences (MELIS), 08003 Barcelona, Spain.

3. Center for Epigenetics and Metabolism, U1233 INSERM, Department of Biological Chemistry, University of California, Irvine, CA 92697, USA.

4. Institute of Neurobiology; Center of Brain, Behavior & Metabolism; University of Lübeck; Lübeck, Germany

5. Department of Biochemistry & Structural Biology, Sam and Ann Barshop Institute for Longevity and Aging Studies, University of Texas Health San Antonio, San Antonio, TX, 78229, USA.

6. Department of Medicine (H7), Karolinska Institute, Stockholm 141 86, Sweden.

7. Department of Biomedical Sciences, Humanitas University, Via Rita Levi Montalcinni 4, 20090 Pieve Emanuele, (Milan), Italy.

8. IRCCS Humanitas Research Hospital, Via Manzoni 56, 20089 Rozzano, (Milan), Italy.

9. Hospital del Mar Research Institute, Cancer Research Programme, 08003, Barcelona, Spain.

10. Catalan Institution for Research and Advanced Studies (ICREA), 08010, Barcelona, Spain.

11. Altos Labs Inc, San Diego Institute of Science, San Diego, CA 92121, USA.

12. Lead contact.

* Correspondence to: thomas.mortimer@irbbarcelona.org; pmunozcanoves@altoslabs.com; pwelz@researchmar.net; salvador.aznar-benitah@irbbarcelona.org

Summary

In mammals, the circadian clock network drives daily rhythms of tissue-specific homeostasis. To dissect daily inter-tissue communication, we constructed a mouse minimal clock network comprising only two nodes: the peripheral epidermal clock and the central brain clock. By transcriptomic and functional characterization of this isolated connection, we identified a gatekeeping function of the peripheral tissue clock with respect to systemic inputs. The epidermal clock concurrently integrates and subverts brain signals to ensure timely execution of epidermal daily physiology. Timely cell cycle termination in the epidermal stem cell compartment depends upon incorporation of clock-driven signals originating from the brain. In contrast, the epidermal clock corrects or outcompetes potentially disruptive feeding-related signals to ensure the optimal timing of DNA replication. Together, we present an approach for cataloguing the systemic dependencies of daily temporal organization in a tissue, and identify an essential gate-keeping function of peripheral circadian clocks that guarantees tissue homeostasis.

Introduction

Consistent and timely execution of homeostatic programs is essential for the long-term maintenance of organismal health[1]. In mammals, many processes that maintain cellular, tissue, and systemic homeostasis exhibit a strict 24-hour periodicity that ensures their optimal alignment to diurnal changes in the internal and external environment [2]. To drive this daily rhythmic physiology, mammals express a circadian clock in almost all cell types that initiates time-of-day and tissue-specific homeostatic processes[3]. Essential in ensuring organism-wide coherence of daily physiology is the body's central clock, located in the hypothalamic suprachiasmatic nucleus (SCN)[4]. The SCN clock directly receives light signals through the retina, which enables it to phase-align with external (solar) time and to subsequently drive neural, hormonal, and behavioral rhythms that synchronize 'peripheral' clocks in other tissues. Complementing this regulatory mechanism, peripheral clocks also receive additional input directly from external cues[5–7], as well as internal signals from other peripheral clocks[8–12]

Communication between the clocks likely relies on subsets of hormones, metabolites, and neural signals, yet the exact nature of these intermediaries remains poorly defined[13]. Furthermore, the mechanisms that allow tissue-relevant signals to be parsed from the milieu of other systemic, micro-environmental and extra-corporeal cues are unclear. Providing answers to these questions is pertinent, as incoherence introduced into this network of clocks through ageing, disease, or lifestyle changes, disrupts the daily homeostatic processes required for maintaining health [2,9,14–16]. Therefore, identifying the specific functions of inter-clock communication pathways is an essential first step towards identifying ways to prevent its desynchronization or rewiring in diseased states.

To date, most studies have relied on disruption of putative signaling nodes (through genetic knockout, environmental interventions, or pharmacological inhibition) to characterize the systemic inputs that control daily tissue physiology[13]. However, these approaches cannot isolate individual clock-driven interactions between tissues, preventing comprehensive cataloguing of the daily physiology that they drive, and the mechanisms by which they do so. To circumvent this, we have reconstructed a minimal clock network *in vivo* constituting only the central clock (brain) and a single peripheral clock defined by the epidermis. This approach allowed us to dissect the specific contributions of a key signaling node (*i.e.,* the central clock) within the network in driving a tissue's daily rhythmic physiology (*i.e*., the epidermis). In doing so, we define in unprecedented detail those rhythmic epidermal processes requiring input from the central clock and those in which the broader network of peripheral clocks (*i.e*., non-brain clocks) are necessary. Concomitantly, and most strikingly, we show that the epidermal clock not only integrates relevant systemic signals, but also gates those that may be detrimental to its

continued homeostasis. Specifically, in proliferating epidermal stem cells, this gatekeeper function of the local clock subverts feeding-related signals that would lead to DNA replication timing that is antiphasic to physiological phase[17–19]. Thus, we propose that peripheral tissue clocks act as gatekeepers to enable selective integration of the systemic signals required to drive daily tissue homeostasis.

Results

Tissue-specific reconstitution of *Bmal1* expression isolates communication between the central (brain) clock and a peripheral (epidermal) clock

We set out to isolate the communication between a key signaling node and a target tissue, to understand the extent to which the node regulates the target tissue´s daily physiology. We elected to focus first on signals generated by the central circadian clock in the brain, given its essential role in controlling the body's network of tissue clocks. As the peripheral tissue receiving these signals, we chose to study the intrafollicular epidermis of the skin, to exploit its extensively characterized daily physiology that becomes rewired during ageing and by different dietary conditions, such as a high-fat diet or caloric restriction[6,19,20].

To isolate brain:epidermal clock communication, we employed our existing mouse model in which tissue-specific expression of a Cre recombinase reconstitutes the endogenous expression of the indispensable core clock component *Bmal1* - and thus clock activity - in an otherwise clock-deficient mouse (herein, *Bmal1*-StopFL mice)[6]. Previously, we showed that keratin 14–Cre-driven reconstitution (RE) of *Bmal1* expression in *Bmal1*-StopFL mice (herein, epi-RE mice) leads to clock activity and a limited daily physiology specifically in the intrafollicular epidermis, i.e., in a tissue-autonomous manner[6]. To determine which epidermal daily physiology functions only rely on receiving brain clock signals (and do not need clock:clock communication), we generated a *Bmal1*-StopFL mouse model that expressed Cre recombinase from the synaptotagmin 10 promoter (*Syt10*-Cre), which is expressed specifically in the brain (with high expression in the SCN)[21], to give brain-reconstituted (brain-RE) mice (Figure 1A). We have recently shown that *Syt10*-Cre-driven *Bmal1* expression in the *Bmal1*-StopFL model is restricted to the brain, where *Bmal1* is expressed in the SCN and other brain regions such as the prefrontal cortex and hippocampus[22]. Importantly, *Syt10*-Cre-driven *Bmal1* expression is sufficient to drive daily cycles of activity, feeding and metabolism at the correct time of day[22], indicating that the SCN clock is correctly reconstituted. Finally, we crossed epi-RE with brain-RE mice, to produce a mouse line with reconstituted clocks in both the epidermis

and the brain/SCN, giving a double-reconstituted (RE/RE) mouse model for studying brain:epidermal clock communication (Figure 1A).

Peripheral clocks, including those in skin, require communication with the brain clock for full entrainment to external conditions[5,23]. To confirm that brain:epidermal clock communication was restored in RE/RE mice, we characterized whether the reconstituted brain clock entrained the epidermal clock. To do so, we first obtained the diurnal epidermal transcriptome from epi-RE, brain-RE, RE/RE, and WT mice (eight-week-old male mice, under a 12h:12h light/dark [LD] cycle). Strikingly, in the epidermis from RE/RE mice, genes of all core components of the epidermal clock, as well as several key clock-controlled genes, including *Dbp, Tef* and *Pdxk*[24–26], oscillated with amplitudes, phases, and periods that were indistinguishable from WT mice (Figure 1B and C). In contrast, and as previously described, oscillation patterns of core clock genes and a subset of clock-controlled genes in epidermis from epi-RE were dampened, as compared to those of WT mice (Figure 1B and 1C)[6,7] , but still present. In brain-RE epidermis, however, significant oscillations were absent for all clock related genes (Figure 1B and 1C), in line with an essential role of BMAL1 in driving the circadian clock in peripheral tissues. Thus, we concluded that our model reconstituted known communication pathways between the brain and peripheral clocks, making it appropriate to elucidate the degree to which the brain clock controls daily epidermal physiology.

Intact daily epidermal physiology requires communication with the brain and other peripheral tissues

Daily epidermal physiology comprises a rhythmic execution of cell cycle, DNA repair, cell differentiation, and metabolic pathways, which together maintain tissue integrity and functionality[2,18–20,27]. Underlying this daily physiology are diurnal oscillations in the expression of thousands of transcripts, which endow rhythmicity to homeostatic processes. As such, we defined diurnal transcriptomes for the epidermis of epi-RE, brain-RE, RE/RE and WT mice to determine the role of brain clock signals in driving daily epidermal physiology. To do so, we applied the rhythmicity detection algorithms JTK_Cycle and BIO_CYCLE (algorithms that use distinct methods of rhythmicity detection)[28,29] to our data sets and then generated consensus diurnal transcriptomes by intersecting the lists of rhythmic genes identified by each algorithm (Figure 1D, S1A and S1B; Supplemental table 1). In line with previous studies[6,19], 2046 genes were rhythmically expressed in WT epidermis (Figure 1D; Supplemental table 1), with a distinct night-time peak in expression (ZT18-24) (Figure S1C and 1D). Moreover, the WT epidermal diurnal transcriptome was enriched

for pathways related to the mitotic cell cycle, protein homeostasis and oxidative metabolism (Figure 1E and 1F; Supplemental table 2) – all key elements of epidermal daily physiology[6,19]. Strikingly, and in contrast to the indistinguishable gene oscillations of their core clock machinery components (Figure 1B and 1C), the diurnal transcriptome of RE/RE epidermis constituted 1093 genes (Figure 1D; Supplemental table 1). This RE/RE diurnal transcriptome lacked enrichment for several biological processes rhythmic in WT epidermis, such as ribosome biogenesis and mitochondrial organization (Figure 1F). However, the RE/RE diurnal transcriptome shared with WT enrichment for pathways related to the cell cycle and vesicle transport (Figure 1E and F; Supplemental table 2). Importantly, this suggested that a significant part of the epidermal daily physiology is recovered upon brain:epidermal clock communication, yet inputs from other clock nodes are required for a complete daily epidermal physiology.

Epi-RE and brain-RE epidermis also exhibited diurnal transcriptomes (343 and 900 genes, respectively) (Figure 1D; Supplemental table 1). This observation agreed with the ability of the epidermal clock to drive autonomously a limited portion of the epidermal diurnal transcriptome[6], and the capacity of the brain clock to impose clock-independent rhythmicity upon peripheral tissues[22]. Interestingly, the diurnal transcriptomes of epi-RE and brain-RE mice were almost exclusively enriched for genes involved in the early cell cycle (G1/S transition, DNA replication) (Figure 1E; Supplemental table 2). This contrasted with the WT and RE/RE diurnal transcriptomes where pathways related to both the late (G2/M transition, cytokinesis) and early cell cycle were present (Figure 1E; Supplemental table 2). Together, this suggested the intriguing possibility that tissue-autonomous and systemic mechanisms can drive rhythms in the early cell cycle, whilst brain:epidermal clock communication is required for physiological rhythmicity of the late cell cycle.

Direct intersection of circadian or diurnal transcriptomes does not allow statistically rigorous identification of gene sets showing equivalent or differing rhythmic expression patterns between experimental conditions[30,31]. Thus, to compare directly the transcriptional rhythms of the different conditions, we applied the algorithm DryR[32] that classifies genes into distinct sets, which share patterns in their rhythmicity parameters between multiple experimental conditions. This enabled us to define with statistical certainty the genes reliant upon different clock communication pathways for their rhythmic expression. DryR identified 629 genes (BICW $\geq$ 0.4, Amp $\geq$ 0.25, Periodicity = 24 hours) rhythmically expressed with similar amplitude and phase in WT and RE/RE epidermis, but not detectably rhythmic in epi-RE or brain-RE (Figure 2A and S1E; Supplemental table 1). That is, the rhythmic expression of these genes required the communication between the brain and the epidermal clocks. Strikingly, and in line with our consensus diurnal transcriptome analysis (Figure

1E), this gene set was almost exclusively enriched for genes involved in the late cell cycle (G2/M checkpoint, mitotic spindle organization, metaphase-anaphase transition) (Figure 2B; Supplemental table 2), strongly suggesting a key role for brain:epidermal clock communication in ensuring timely cell cycle termination. This included essential regulators of the G2/M transition (*Cdk1*, *Ccnb1*, and *Ccnb2*), and of mitotic spindle formation (*Aurka*, *Cdc20* and *Cenpa*) (Figure 2C). Amongst brain:epidermal clock communication regulated genes, known targets of the G2/M master regulator FOXM1[33] were strongly enriched (Figure 2D), and concordantly, *Foxm1* was rhythmically expressed only in WT and RE/RE epidermis (Figure S1F). FOXM1 is proposed to mediate circadian regulation of the late cell cycle[34], and thus brain clock signals may synergize with the epidermal clock to regulate this factor. *Ccnb1* (Cyclin B1), which has been previously identified as a key circadian regulatory node of the cell cycle[35], was also rhythmically expressed only in WT and RE/RE epidermis, suggesting an alternative or complementary point of regulation. We thus concluded that correct timing of late cell cycle execution likely relies on brain:epidermal clock communication.

A further 399 genes were rhythmically expressed only in WT epidermis, i.e., they required inputs from other peripheral clocks (Figure 2E and S1G; Supplemental table 1). Contrasting with those regulated by brain:epidermal clock communication, this gene set was enriched for pathways of ribosome biogenesis and maintenance of the extracellular matrix (ECM) (Figure 2F; Supplemental table 2). This included the processing machinery of ribosomal RNAs (*Bop1*, *Exosc6*, *Nol9*) and ECM proteins required to build the epidermal basement membrane (*Col4a1*, *Col5a1*, *Fbnl1*) (Figure 2G). An intact basement membrane is required to ensure correctly executed keratinocyte differentiation[36], suggesting that peripheral clock input to the epidermis guarantees faithful cell fate commitment by maintaining basement membrane homeostasis. Transcription factor (TF) binding analysis revealed significant enrichment for MYC, MAX and CREB1 targets amongst peripheral clock-induced rhythmic genes (Figure S1H); a set of TFs distinct to those mediating brain:epidermal communication (Figure 2D). The MYC-MAX complex negatively regulates keratinocyte expression of ECM components[37], and could offer a means for peripheral:epidermal clock communication to modulate ECM composition and interactions.

To establish the necessity of peripheral clock inputs to maintain epidermal homeostasis, we performed differential expression analysis comparing the transcriptomes of WT and RE/RE epidermis irrespective of time-of-day. We identified 333 differentially expressed genes (DEGs) (Padj ≤ 0.05, FC ≥ 1.5), with the majority of genes upregulated in WT relative to RE/RE epidermis (10 downregulated, 323 upregulated) (Supplemental table 1). Importantly, DEGs were most highly enriched for pathways related to assembly and maintenance of the dermal ECM (Figure 2H;

Supplemental table 2), with further enrichment for pathways involved in cell motility, organ development and FGF signaling. We therefore concluded that the peripheral clock inputs play an essential role in guaranteeing correct execution of epidermal daily physiology, with a particular importance in ensuring maintenance of ECM homeostasis.

Our strategy to detect gene expression rhythmicity meant that any differences in inter-individual phase alignment between conditions could affect the relative number of rhythmically expressed genes detected, and thus our conclusions relating to clock:clock communication. This possibility is testable, as any differences in inter-individual phase alignment would give rise to differences in gene expression variance (due to a phase dispersion of biological replicates) between conditions, specifically for commonly rhythmic genes. However, data from our previous work [6], and analysis of gene expression variances across biological replicates, suggested that inter-individual phase alignment does not differ between clock reconstitution conditions (Figure S2A-B). Moreover, although generally (in all expressed genes, irrespective of rhythmicity) standard deviation of gene expression is significantly increased in RE conditions vs WT (Figure S2C), the change is minimal (3-6%), indicating that differences in biological variability do not meaningfully distinguish the conditions. Thus, differences in clock:clock communication pathways are the most likely explanation for the distinct rhythmic expression patterns observed in each clock reconstitution condition.

In principle, clock:clock communication may drive epidermal expression rhythms: i) by inducing rhythms in individual epidermal cells, ii) by inducing phase coherence between already rhythmic epidermal cells. Arguing that peripheral:epidermal clock communication does not act by inducing intra-tissue phase coherence (ii), there was no significant difference between the amplitudes of consensus rhythmic transcriptomes (Figure S2D) or core clock genes (Figure S2E) in RE/RE and WT epidermis. Nonetheless, the amplitude of the consensus rhythmic transcriptomes of epi-RE and brain-RE epidermis, and the amplitude of the epi-RE core clock, were significantly decreased relative to WT (Figure S2B and 1B). Thus, both induction of rhythmicity in individual cells (i) and intra-tissue coherence (ii) may be driven by brain:epidermal clock communication, whilst induction of rhythmicity in individual cells (i) is likely the primary output of peripheral:epidermis clock communication.

To explore further the potential mechanisms underlying clock communication, we categorized each class of rhythmic genes by their expression magnitudes in each condition. The majority of genes requiring brain:epidermal clock communication, segregated into two classes: i) equivalent mean expression in all conditions (211 genes) (Figure S3A and B); ii) equivalent mean expression in WT, RE/RE and epi-RE, but decreased or increased expression in brain-RE (205 genes) (Figure S3C and

D). Strikingly, genes equivalently expressed in all conditions (i) were enriched for pathways related to the late cell cycle, indicating that rhythmicity of this process is restored by imposing rhythmicity upon genes already expressed in the cell (Figure S3B).

Analysis of genes requiring peripheral:epidermal clock communication for their rhythmicity identified two expression profiles describing the majority of genes: i) equivalent mean expression in all conditions (166 genes) (Figure S3E); ii) higher expression in WT relative to all other conditions (77 genes) (Figure S3G). Those with equivalent mean expression (i) were enriched for terms related to ribosome biogenesis (Figure S3F), but, in contrast, genes upregulated in WT (2) were enriched for extra cellular matrix terms (Figure S3H). This suggested that regaining rhythmicity of ribosome biogenesis required imposing rhythmicity upon already expressed genes, whilst for ECM-related processes a dual upregulation and gain of rhythmicity is required.

The epidermal clock selectively gates brain clock signals

In mice, epidermal DNA replication peaks during the night, ostensibly to avoid exposing the vulnerable replicating DNA to the daytime peak of DNA-damaging oxidative conditions[17,18,38]. Our data indicated that both the local epidermal clock and brain clock are able to independently drive rhythms in this key aspect of daily epidermal physiology (Figure 1E), thus we set out to characterize further this apparent dual regulation. In doing so, we identified in our DryR analysis a commonly rhythmic set of 119 genes (Supplemental table 1) that was highly enriched for pathways related to the early cell cycle and DNA replication (Figure 3A and 3C; Supplemental table 2). Most strikingly, although these genes were rhythmically expressed in WT, RE/RE, epi-RE and brain-RE epidermis, their expression was entirely antiphasic in brain-RE relative to the other conditions (Figure 3B). While transcript expression peaked at the beginning of night-time (ZT10-14) in WT, RE/RE, and epi-RE mice, it peaked around day-time onset (ZT22-2) when only the brain clock was present (brain-RE). Thus, when working alone, the brain clock appeared to drive a peak in DNA replication in proliferative epidermal stem cells that coincided with the timing of maximum oxidative metabolism in the epidermis[17]. Critically, however, when both the local epidermal clock and brain clock were present (RE/RE epidermis), the local clock was able to gate signals from the brain clock (Figure 3A and 3B), generating WT-phased expression rhythms. Genes exhibiting antiphasic expression included indispensable components of the DNA replication machinery, such as those encoding *Mcm2-4*, *Gins2*, *Pcna*, and *Pole* (Figure 3D), and core regulators of the early cell cycle *Cdk2*, *Ccne1*, *E2f1* and *Cdc45* (Figure 3E). Importantly, comparison with existing data from Welz *et al.* (2019) showed that only 2

of the 119 genes oscillated in the epidermis of whole-body *Bmal1*-knockout mice kept under LD conditions (*Bmal1*-KO) (Figure S1I), confirming the reliance of the other genes on either local or brain clock activity for oscillatory expression of the DNA replication machinery. The existence of WT-phased rhythms in epi-RE epidermis (Figure 3A), suggested that the epidermis clock can autonomously drive diurnal expression rhythms of DNA replication pathways. As such, the gating of brain clock signals by the epidermal clock may be either competitive, with both mechanisms coexisting and the epidermal clock dominating, or, alternatively, the epidermal clock may actively correct aberrant brain-clock signals determining timing of DNA replication. Together, this suggested that the epidermal clock is essential for gating signals originating from the brain clock, which would otherwise compromise the physiological phase of daily rhythms in DNA replication.

To functionally validate the apparent gating capacity of the epidermal clock, we quantified the proportion of proliferating epidermal stem cells undertaking each phase of the cell cycle across the day by FACS analysis in all conditions (8-week-old male mice, LD). As previously observed[18,19], WT mice showed a robust night-time peak (ZT16-20) and daytime trough (ZT4-8) of epidermal DNA replication (Figure 4A), whilst *Bmal1*-KO mice were arrhythmic (Figure 4A). Similarly, and as predicted by the transcriptional data, Epi-RE mice showed physiologically phased rhythms of epidermal DNA replication (Figure 4A). In contrast, DNA replication rhythms in brain-RE epidermis were antiphasic (ZT4-8 peak) with respect to WT (Figure 4A), an observation we independently confirmed by *in vivo* monitoring of DNA replication via EdU staining (Figure S4A-B). Crucially, this antiphasic pattern was corrected in RE/RE epidermis to generate WT-like rhythms of DNA replication (Figure 4A), thus confirming the ability of the local epidermal clock to gate potentially detrimental brain clock signals. Although we observed distinct rhythms in the proportion of epidermal cells executing S phase, the proportion of cells proliferating was not rhythmic (Figure S4C) and overall levels did not differ between the conditions (Figure S4D). Thus, our results confirmed that the epidermal clock gates brain clock signals to ensure timely execution of DNA replication.

Our transcriptional analyses also predicted that brain:epidermal clock communication ensured the timely execution of the late cell cycle (Figure 1E and 2B). In agreement, WT and RE/RE epidermis showed coherent rhythms in the proportion of cells present in G2/M phases (2n DNA content) (Figure 4B) and timing of mitotic division (observed as a sharp decrease in cells with a 2n DNA content at ZT4-8) (Figure 4B). This contrasted with epi-RE and brain-RE mice, which exhibited non-significant dampened and antiphasic rhythmicity patterns of late cell cycle execution, respectively (Figure 4B).

The epidermal clock gates brain-driven feeding signals to ensure correctly timed DNA replication

Regulation of peripheral tissue daily physiology by the brain clock may occur via direct cues (e.g., endocrine, neuronal), or indirect signals resulting from body temperature rhythms, feeding-fasting cycles or other secondary molecular rhythms in peripheral tissues. In particular, feeding-related signals instruct and synergize with the core clock machinery of peripheral tissues to guarantee timely execution of daily physiology[11,39]. However, the central and lung clocks are refractory to changes in feeding cycles, indicating that in certain tissues mechanisms may exist to inhibit the effects of feeding-related signals upon tissue daily physiology[12,40]. Moreover, feeding-derived metabolites and insulin signaling are potent regulators of the cell cycle[41,42]. We therefore hypothesized that the epidermal clock could be gating feeding-fasting signals to prevent aberrant timing of DNA replication. If true, reinstating normal feeding cycles (through night feeding) in clock-less animals should lead to antiphasic timing of DNA replication due to the lack of a corrective epidermal clock. Indeed, night-time feeding (2-weeks, food available ZT12-ZT0) of *Bmal1*-KO mice induced a trend towards antiphasic rhythmicity in epidermal DNA replication relative to WT (Figure 4C). In contrast, day feeding of *Bmal1*-KO mice (2-weeks, food available ZT0-ZT12) led to a night-time peak in DNA replication (Figure 4C), indicating that epidermal cell cycle initiation is generally entrainable by feeding cycles in the absence of a functional epidermal clock, but to a non-physiological phase. Importantly, day feeding of brain-RE mice, which mainly feed during the night under *ad libitum* conditions, corrected the antiphasic pattern of DNA replication observed under *ad libitum* conditions (Figure 4C), in line with feeding cycles serving as the brain clock signal driving antiphasic rhythms. However, most significantly, epi-RE mice, which show no daily feeding rhythms under *ad libitum* conditions[6], maintained a WT-like phase of DNA replication when night feeding was imposed (Figure 4C), demonstrating the capacity of the epidermal clock to gate feeding-related signals. Together, we concluded that the local epidermal clock gates brain clock-generated feeding-fasting signals to ensure timely initiation of DNA replication in proliferating epidermal stem cells (Figure 4D).

Epidermal clock gating as a physiologically relevant process

Our comparative analysis of different clock-reconstituted models suggested that the epidermal clock gates systemic signals to regulate epidermal daily physiology. However, the extent to which this functionality exists in the physiological state remained unclear. To explore whether the epidermal clock gates extracellular signals in the context of a fully functional clock network, we turned to our

previously published mouse model[43] in which a K14-Cre drives conditional *Bmal1* deletion in the epidermis (epi-Bmal1KO). Here, we predicted that loss of epidermal clock gating should lead to the emergence of non-physiological rhythms of epidermal processes, driven by now ungated extracellular signaling pathways. To test this, we generated a diurnal epidermal transcriptome of epi-Bmal1KO mice (eight-week-old male mice, under a 12h:12h LD cycle) and performed a DryR differential rhythmicity analysis comparing the epi-Bmal1KO diurnal transcriptome with that of our existing WT control. As expected, core clock and clock-output gene expression were arrhythmic in the epidermis of epi-Bmal1KO animals, confirming the abolishment of local clock activity (Figure S5A and S5B).

To our surprise, genes rhythmic in WT epidermis (323 genes, DryR analysis), but not in the epi-Bmal1KO epidermis, were enriched for pathways related to the early cell cycle (Figure S5C and S5D), i.e., these genes required activity of the epidermal clock for their rhythmic expression. This contrasted with brain-RE epidermis, where brain clock signals alone were sufficient to drive detectable antiphasic expression rhythms of this pathway (Figure 3A, 3B and 3C). However, visual inspection revealed that key regulators of the early cell cycle, such as *Cdk2*, *E2f1* and *Pole*, shared a marked expression trough at ZT12 (Figure 5A); the time at which expression peaks in WT epidermis. In fact, almost all genes antiphasically expressed in brain-RE epidermis relative to WT (Figure 3A) exhibited an expression trough at ZT12 in epi-Bmal1KO epidermis (Figure 5B). This suggested that when the epidermal clock is absent, extracellular signals, most likely originating from the brain clock, repress early cell cycle gene expression even in the presence of an otherwise intact clock network. Thus, we concluded that the epidermal clock gates extracellular signals that would otherwise repress epidermal expression of early cell cycle genes in an untimely manner.

Further evidencing epidermal clock gating, we identified 234 genes rhythmic in both conditions, but with a 4-8 hour phase delay in epi-Bmal1KO epidermis, which were enriched exclusively for late cell cycle pathways (Figure S5E, 5C, 5D and 5E). The absence of similar rhythms in brain-RE epidermis suggested that peripheral clocks inputs were driving these rhythms in epi-Bmal1KO epidermis. As such, in the physiological state the epidermal clock gates extracellular signals that would otherwise: i) induce a daily punctual repression of early cell cycle regulator expression in an untimely manner, ii) drive rhythmic expression of late cell cycle regulators, but with a 4-8 phase delay relative to WT epidermis. To understand whether these aberrant transcriptional rhythms affected execution of the epidermal cell cycle, we quantified in epi-Bmal1KO epidermis the proportion of proliferating epidermal stem cells undertaking each phase of the cell cycle across the day by FACS analysis (8-week-old male mice, 12h:12h LD). K14-Cre-driven deletion of *Bmal1* in the epidermis led to a distinct peak in epidermal cells performing DNA replication at ZT2, representing a 6-hour phase

delay relative to WT epidermis (Figure 5F). Similarly, execution of the late cell cycle (G2/M phases) was also rhythmic in epi-Bmal1KO, yet phase delayed by 6 hours relative to WT mice (Figure 5F). Thus, epidermal clock gating of brain and peripheral clock inputs is required to ensure the correctly phased execution of the full cell cycle.

Despite the absence of a functional epidermal clock, we identified a further 739 genes that had equivalent rhythmic expression in WT and epi-Bmal1KO epidermis (Figure 5G). This gene set was exclusively enriched for GO terms related to ribosome biogenesis (Figure 5H and 5I) - the very same pathway our RE models identified as requiring peripheral clock input to drive diurnal rhythmicity (Figure 2F). We thus concluded that signals emanating from other peripheral clocks induce transcriptional rhythms of ribosome biogenesis in the epidermis independently of the epidermal clock.

Brain clock communication ensures robust epidermal daily physiology in the absence of light cues

Robustness against short-term variations in environmental conditions is essential for maintaining a consistent daily physiology. Signals from the autonomously oscillating brain clock are key for ensuring correctly timed execution of daily physiology even when environmental cues are acutely disrupted or absent[5,44]. However, it is unknown whether the brain clock alone is sufficient for this stabilizing function, or if cooperation with other elements of the clock network are also required. To define the sufficiency of brain clock communication in endowing stability to daily physiology in peripheral tissues, we characterized the epidermal circadian transcriptome in WT, RE/RE, epi-RE, and brain-RE mice (8-week-old females) in the absence of normal light/dark cycles (i.e., after one week of constant darkness) (Figure S6A). Despite the absence of light cues, core clock genes oscillated identically in epidermis from WT and RE/RE mice in dark/dark (DD) conditions (Figure 6A), demonstrating that communication with the brain clock alone is sufficient to ensure a stable epidermal clock entrainment. Moreover, the rhythmicity of the clock-output genes *Dbp, Tef*, and *Pdxk* was indistinguishable in epidermis from WT mice and RE/RE mice, further confirming the presence of a WT-like core clock activity in RE/RE epidermis (Figure 6B). In contrast, both core clock and clock output genes lacked rhythmicity in epi-RE epidermis (Figure 6A and 6B), in line with the observation that the autonomous epidermal clock requires light signals for its entrainment[19]. Thus, we concluded that the brain:epidermal clock communication represents a stable and sufficient communication pathway for driving epidermal clock entrainment even in the absence of a rhythmic light cycle.

Deriving consensus circadian transcriptomes for each condition revealed that WT mice (1781 genes) and RE/RE mice (1042 genes) maintained substantial epidermal circadian transcriptomes in DD conditions, whilst epi-RE mice (45 genes) and brain-RE mice (283 genes) exhibited negligible and limited rhythmicity, respectively (Figure 6C, S6B, S6C, S6D and S6E; Supplemental table 1). Importantly, the RE/RE and WT circadian transcriptomes shared an enrichment for genes related to both the early and late cell cycle (as in male mice under LD conditions) (Figure 6D; Supplemental table 2), whereas that of brain-RE mice was enriched only for the early cell cycle (Figure 6D; Supplemental table 2). As expected, no enrichment of cell cycle regulators was observed in epi-RE in the absence of a rhythmic light cycle (Figure 6D; Supplemental table 2)[6]. DryR analysis identified 911 genes with equivalent rhythmicity in WT and RE/RE epidermis, but arrhythmic in epi-RE or brain-RE (Figure 6E and S6F; Supplemental table 1), i.e., brain:epidermal clock communication regulated under DD conditions. Pathways enriched amongst this gene set included the late cell cycle (Figure 6F; Supplemental table 2), further suggesting that brain:epidermal clock communication maintains physiological rhythms of late cell cycle execution even in the absence of entraining light signals. Once again, this encompassed core regulators of the G2/M transition and mitotic spindle formation *Ccnb1-2*, *Cdc20* and *Cenpe* (Figure 6G and S6G).

Under DD conditions, the epidermal clock continued to gate brain clock signals to ensure timely epidermal DNA replication. DryR identified 89 genes rhythmically expressed in WT, RE/RE, and brain-RE epidermis that were highly enriched for pathways involved in the early cell cycle (Figure 6H and 6I; Supplemental table 1 and 2), but were expressed with an antiphasic rhythm in brain-RE epidermis (Figure 6H and S6H). Again, this included genes encoding core regulators of the early cell cycle, such as *Cdk2* and *E2f1*, and key components of the DNA replication machinery, such as *Mcm2-3*, *Pole*, and *Gins2* (Figure 6J and S6I). Together, these results demonstrated that brain clock signals regulating the epidermal cell cycle are circadian in nature, and confirmed that the local epidermal clock must both integrate and gate distinct systemic signals to ensure correct daily rhythms of the cell cycle.

Discussion

By isolating the communication between two tissue circadian clocks, we have comprehensively dissected the role of a specific signaling node in defining and coordinating a distal tissue's daily physiology. For the brain:epidermal clock communication axis, we show that this connection is sufficient to drive epidermal clock entrainment as well as for specific rhythmic homeostatic

processes, yet, importantly, it is insufficient to ensure full daily physiology. In other words, these additional functions require input from other peripheral clocks, and therefore circadian communication with niche cells or other peripheral tissues is essential for attaining a complete daily physiology. In this sense, growing evidence suggests that peripheral clock communication is a conserved motif across tissue types and organ systems [8–13]. For instance, recent studies suggest that extensive communication may exist between the clocks of metabolic tissues, such as the liver and skeletal muscle, as well as between distinct cell types within individual tissues, such as the liver[8,9,11,12]. This reliance upon input from other peripheral clocks supports the proposed federated structure of the clock network[13], in which each clock receives and consolidates diverse inputs from the environment, the central clock of the SCN, and other peripheral clocks to determine its daily physiology.

Directly contrasting with the systemic dependencies of epidermal daily physiology, we have also demonstrated a gating function of peripheral tissues towards daily brain signals. In particular, we show that the epidermal cell cycle represents a paradigm for cooperation and conflict between the brain and peripheral clocks. If unchecked by the local epidermal clock, feeding-related signals, driven by the brain clock, would induce a morning peak in DNA replication — a profile antiphasic to that of WT epidermis. However, the presence of the local clock suppresses or outcompetes this feeding-related signal and corrects the phase of DNA replication. This interaction suggests that the epidermal clock selectively suppresses systemic signals that would otherwise compromise the coherence of homeostatic processes. In direct contrast with the early cell cycle, we also show that brain:epidermal clock communication is sufficient to ensure physiological rhythmicity in execution of late cell cycle stages (G2/M transition and cytokinesis). These distinct interactions between brain clock signals and the early and late stages of the epidermal cell cycle suggest that each stage requires coherence to distinct external events, for which the brain clock signals suffice only in the case of the late cell cycle.

The temporal separation of peak oxidative phosphorylation and peak DNA replication in the epidermis has led to the proposal that the two processes are segregated by the circadian clock to avoid oxidative damage to replicating DNA[17]. Nonetheless, definitive experiments functionally linking these cell states are lacking. Notably, cell proliferation is highly dependent upon aerobic glycolysis to provide the building blocks necessary for faithful cell cycle execution[45]. Thus, a plausible alternative is that a night-time peak in DNA replication may anticipate an enhanced nocturnal availability of glucose, due to feeding activity, which in turn could be used for aerobic glycolysis.

Feeding rhythms, with their established function in entraining most peripheral clocks, are a key central clock-controlled input to peripheral tissue clocks. Emphasizing this importance, approximately 20% of liver daily physiology relies on liver clock integration of feeding signals, and

feeding rhythms are sufficient for nearly 60% of the circulatory metabolite rhythms essential for inter-tissue coordination[11,22]. Feeding also allows coordination within the peripheral clock network, in part by enabling cooperation between liver and muscle clocks in systemic glucose tolerance [8]. Here, we reveal a potentially detrimental side to feeding cycles, showing their capacity to induce untimely activation of biological processes, such as the epidermal cell cycle, when not buffered/gated by peripheral clocks. Although indispensable, daily feeding rhythms may represent a recurrent stress for many tissues, which if left unchecked could lead to loss of coherence in key homeostatic processes and progressive deterioration of tissue integrity. Thus, tissues may be obliged to employ molecular buffers, such as the circadian clock, to neutralize the effects of this daily change in their external environment.

Bodily tissues exist within the context of an ever-changing milieu of extracellular signals, of which only a select few are integrated by cells to maintain tissue homeostasis. Contributing to this dynamic extracellular environment, the body's central clock produces an array of signals that exert essential tasks, such as entraining the rest of the body to changes in light; however, the myriad signals emanating from the brain clock are not universally relevant to the many tissues upon which they impinge. As such, peripheral tissues must selectively interpret and subvert systemic signals originating from the brain clock (and potentially other peripheral clocks), depending on their relevance for correct execution of that tissue's daily physiology (e.g., epidermal DNA replication). To parse the extracellular environment, we propose that tissues employ their circadian clock as a gatekeeper to interpret, buffer and/or correct this complex array of signals (Figure 4D). Supporting such a gating function, peripheral clocks respond differentially to entraining signals, such as feeding and light, implying tissue-specific mechanisms that integrate or suppress particular brain clock signals[12,40]. Moreover, the tissue clocks of liver and muscle are able to inhibit the response of specific peripheral clocks to feeding-related signals[11,12]. Here, we unify these findings, demonstrating the local clock to be both a transducer and repressor of systemic signals.

The rewiring and decay of inter-tissue communication is a recurrent feature of many disease states and during aging[9,46,47]. As such, we believe that our findings represent a critical shift in how circadian clock network function can be understood in the context of both health and disease.

Limitations of Study

The epidermal early cell cycle of epi-RE mice is rhythmic with a WT-phase under LD conditions, indicating that the epidermal autonomous clock alone is able to drive physiologically phased early

cell cycle rhythmicity. This observation, and the ability of the brain clock to induce an antiphasic early cell cycle rhythmicity implies a situation in which, under WT conditions, there coexists a competition between: i) brain-derived signals, ii) the autonomous epidermal clock, to define the phase of the early cell cycle. As such, to 'gate' the early cell cycle the epidermal clock must either outcompete or correct the signals coming from the brain clock to ensure a physiological phase. With the experiments performed in this study, we are unable to distinguish between these two possible mechanisms.

Given the established linkage between the circadian clock and the cell cycle circadian rhythms[48], we believe that a clock-dependent role of BMAL1 is the most likely explanation for reconstituted early cell cycle rhythmicity in epi-RE epidermis under LD conditions. However, it is conceivable that independently of the core clock, re-expression of *Bmal1* cooperates with light cycle signals to drive cell cycle and other epidermal rhythms that we observe. Distinguishing clock-dependent from clock-independent roles of core clock proteins remains a pervasive challenge for the circadian field, and this limitation should be taken into account when interpreting our results.

Acknowledgements

We thank the genomics units at the CNAG and CRG for assistance with RNA sequencing, Prof. Gregor Eichele for generously providing us with the *Syt10*-Cre mice, and Veronica Raker for proofreading the manuscript. The authors acknowledge the following funding sources: **SAB** - European Research Council under the European Union's Horizon 2020 (H2020) research and innovation programme (Grant agreement No. 787041), the Government of Cataluña (SGR grant), the Government of Spain (MINECO) and the Foundation Lilliane Bettencourt. **The IRB Barcelona** is a Severo Ochoa Center of Excellence (MINECO award SEV-2015-0505). **CMG** - H2020 research and innovation programme under the Marie Sklodowska-Curie grant agreement 749869. **KBK** - NIH F32 (Fellowship DK121425). **PMC** - MICINN-RTI2018-096068, ERC-2016-AdG-741966, LaCaixa-HEALTH-HR17-00040, MDA, UPGRADE-H2020-825825, AFM, DPP-Spain, Fundació La MaratóTV3-80/19-202021, MWRF, and María-de-Maeztu Program for Units of Excellence to UPF (MDM-2014-0370) and the Severo- Ochoa Program for Centers of Excellence to CNIC (SEV-2015-0505). **PP** - Wenner-Gren foundations, The foundation Blanceflor, Tore Nilsons foundation and the Novo Nordisk foundation. **PSW** - RYC2019-026661-I funded by MCIN/AEI/10.13039/501100011033, "ESF Investing in your future", PID2020-113317RA-I00 funded by MCIN/AEI/ 10.13039/501100011033, and by the BBVA Foundation. **TM** - H2020

research and innovation programme under the Marie Skłodowska-Curie grant agreement No. 754510. **VMZ** - "la Caixa" INPhINIT Fellowship Grant for Doctoral Studies at Spanish Research Centers of Excellence, "la Caixa" Foundation, Barcelona (ID 100010434, fellowship LCF/BQ/IN17/11620018). The project has received funding from the H2020 research and innovation program (Marie Skłodowska-Curie grant agreement no. 713673). **HO** - the German Research Foundation (DFG) - CRC296/TP13.

Author Contributions

TM, VMZ, PSW and SAB designed the study with critical input from all other authors. TM, VMZ and MA performed the majority of experiments. GP and EG provided experimental assistance with the analysis of the cell cycle by FACS. TM, VMZ, CL and OD performed the data analysis of the diurnal and circadian transcriptomes. PSW and SF generated the *Bmal1*-StopFL mice used in this study. TM and SAB wrote the manuscript, integrating feedback from all other authors.

Declaration of interests

SAB is a co-founder and scientific advisor of ONA Therapeutics. PMC is an employee of Altos Laboratories.

Main figure titles and legends

Figure 1 - Tissue-specific reconstitution of *Bmal1* expression isolates communication between the epidermal clock and brain clock:

(A) The *Bmal1*-StopFL mouse[6] (left) and the breeding procedure used to generate the RE/RE model (right). The image was created using biorender.com. (**B** and **C**) Diurnal expression patterns of core clock (B) and clock-controlled genes (C) in the epidermis of all clock reconstitution conditions (RNA-seq). Values = $\log_2$-transformed mean RPKM of four biological replicates (± standard deviation). ZT0 is double-plotted. (**D**) Quantification of the epidermal diurnal transcriptome in each clock reconstitution condition. (**E** and **F**) Selected Gene Ontology terms enriched amongst the diurnal transcriptomes of epidermis from different clock reconstitution conditions (E) (cell cycle–related), or only in the diurnal transcriptome of WT epidermis, but not other clock reconstitution conditions (F).

RPKM, reads per kilobase per million mapped reads; SCN, suprachiasmatic nucleus; Syt10, synaptotagmin 10; ZT, *Zeitgeber* time. See also Figure S1, S2, S3, and Supplemental table 1 and 2.

Figure 2 – Communication with brain and other peripheral tissues ensures intact daily epidermal physiology:

(**A** and **E**) Heat maps showing the diurnal expression patterns of genes equivalently rhythmic only in WT and RE/RE epidermis (629 genes) (A) or rhythmic only in WT epidermis (399 genes) (E), in all clock reconstitution conditions. (**B** and **F**) Selected Gene Ontology and Reactome terms enriched amongst genes with equivalent rhythmic expression only in WT and RE/RE epidermis (B) (see A) or rhythmic only in WT epidermis (F) (see E). (**C** and **G**) Diurnal expression patterns of late cell cycle regulators (C) and extracellular membrane/ribosome components (G) in the epidermis of each clock reconstitution condition (RNA-seq). Values = $\log_2$-transformed mean RPKM of four biological replicates (± standard deviation). ZT0 is double-plotted. (**D**) Enrichment of consensus transcription factor targets (identified in ChEA and ENCODE) amongst genes equivalently rhythmic in WT and RE/RE only (see A). (**H**) Selected Gene Ontology terms enriched amongst genes differentially expressed between WT and RE/RE epidermis, irrespective of time-of-day. ChEA, ChIP Enrichment Analysis; ENCODE, Encyclopedia of DNA Elements; RPKM, reads per kilobase per million mapped reads; ZT, *Zeitgeber* time. See also Figure S1, S2, S3, and Supplemental table 1 and 2.

Figure 3 - Brain clock signals drive an antiphasic pattern of epidermal DNA replication:

(**A**) Heat map showing the diurnal expression patterns of genes with antiphasic rhythmicity in brain-RE epidermis relative to all other clock reconstitution conditions (119 genes), in all clock reconstitution conditions. (**B**) Circular histograms indicating the expression phases of brain-RE antiphasic genes (see A) relative to all other clock reconstitution conditions. (**C**) Selected Gene Ontology and Reactome terms enriched amongst brain-RE antiphasic genes (see A). (**D** and **E**) Diurnal expression patterns of the DNA replication machinery (D) and early cell cycle regulators (E) in the epidermis of each clock reconstitution condition (RNA-seq). Values = $\log_2$-transformed mean RPKM of $n = 4$ biological replicates (± standard deviation). ZT0 is double-plotted. RPKM, reads per kilobase per million mapped reads; ZT, *Zeitgeber* time. See also Figure S1, and Supplemental table 1 and 2.

Figure 4 - The epidermal clock corrects feeding signals to ensure physiologically phased DNA replication:

(**A** and **B**) Percentage of actively cycling epidermal cells (Ki67-positive) in S (> 1n - < 2n DNA content) or G2/M phase (2n DNA content) across a 24-hour cycle. Values = mean of n = 4-8 biological replicates (± standard deviation). ZT0 is double-plotted. *P* and phase 'peak' values were calculated using JTK_Cycle. (**C**) Percentage of actively cycling epidermal cells (Ki67-positive) in S phase (> 1n - < 2n DNA content) at ZT4 and ZT16, after two weeks exposure to different feeding regimes. Values = mean of n = 4-8 biological replicates (± standard deviation). (**D**) Graphical representation of gating of extracellular signals by the epidermal clock. ZT, *Zeitgeber* time. See also Figure S4.

Figure 5 – The epidermal clock gates extracellular signaling inputs in the physiological state:

(**A, E** and **I)** Diurnal expression patterns of early cell cycle (A), late cell cycle (E) and ribosome biogenesis (I) regulators in the epidermis of wild-type and epi-Bmal1KO epidermis (RNA-seq). Values = $\log_2$-transformed mean RPKM of n = 4 biological replicates (± standard deviation). ZT0 is double-plotted. **(B** and **G)** Heat map showing the circadian expression patterns of genes with an antiphasic expression rhythm in brain-RE epidermis (119 genes) (B) or with equivalent rhythmicity in wild-type and epi-Bmal1KO epidermis (739 genes) (G), in wild-type and epi-Bmal1KO epidermis. **(C)** Circular histograms indicating the expression phases of genes rhythmic in wild-type and epi-Bmal1KO epidermis, but phase shift in epi-Bmal1KO. **(D** and **H)** Selected Gene Ontology and Reactome terms enriched amongst genes rhythmic in wild-type and epi-Bmal1KO epidermis, but phase shifted in epi-Bmal1KO (D) and genes equivalently rhythmic in wild-type and epi-Bmal1KO epidermis (H). **(F)** Percentage of actively cycling epidermal cells (Ki67-positive) in S (> 1n - < 2n DNA content) or G2/M phase (2n DNA content) across a 24-hour cycle. Values = mean of n = 4-5 biological replicates (± standard deviation). ZT0 is double-plotted. RPKM, reads per kilobase per million mapped reads; ZT, *Zeitgeber* time. See also Figure S5.

Figure 6 - Brain clock communication ensures robust daily epidermal physiology in constant darkness:

(**A** and **B**) Circadian expression patterns of core clock genes (A) and clock-controlled genes (B) in the epidermis of all clock reconstitution conditions (RNA-seq). (**C**) Quantification of the epidermal

circadian transcriptome in each clock reconstitution condition. (**D**) Selected Gene Ontology terms (cell cycle–related) enriched amongst the circadian transcriptomes of epidermis from different clock reconstitution conditions. (**E** and **H**) Heat map showing the circadian expression patterns of genes equivalently rhythmic only in WT and RE/RE epidermis (961 genes) (E) or with antiphasic rhythmicity in brain-RE epidermis relative to WT and RE/RE (89 genes), in all clock reconstitution conditions. (**F** and **I**) Selected Gene Ontology and Reactome terms enriched amongst genes rhythmically expressed only in WT and RE/RE epidermis (F) (see E) or antiphasic in brain-RE epidermis (I) (see H). (**G** and **J**) Circadian expression patterns of the late cell cycle (G) and early cell cycle regulators (J) in the epidermis of each clock reconstitution condition (RNA-seq). In (A), (B), (G) and (J), values represent the $\log_2$-transformed mean RPKM of $n = 4$ biological replicates (± standard deviation), and CT0 is double-plotted. RPKM, reads per kilobase per million mapped reads. See also Figure S6, and Supplemental table 1 and 2.

STAR Methods

Lead Contact

Further information and requests for resources and reagents should be directed to and will be fulfilled by the lead contact, Salvador Aznar Benitah (salvador.aznar-benitah@irbbarcelona.org).

Materials Availability

All unique/stable reagents generated in this study are available from the lead contact with a completed material transfer agreement.

Data and Code Availability

RNA-seq data have been deposited at the Gene Expression Omnibus and are publicly available as of the date of publication. Accession numbers are listed in the key resources table. No custom code was generated in this study. Any additional information required to reanalyze the data reported in this paper is available from the lead contact upon request.

EXPERIMENTAL MODEL AND SUBJECT DETAILS

Housing of mice and study design

All mice were bred and maintained in the animal facilities of the Barcelona Science Park (PCB), following the applicable Spanish and European Union regulations. The experimental protocols applied in this paper were approved by the Catalan Government, in line with the relevant legislation and the guidelines of the Institutional Animal Care and Use Committee (IACUC) at the PCB.

The ARRIVE guidelines for reporting and performing animal experiments[49] were taken into consideration during the design of all experiments. Mice were maintained in rooms at 22°C degrees with *ad libitum* access to standard chow diet, except for feeding-related experiments, where feed was available from ZT12-0 (night feeding) and ZT0-12 (day feeding). To profile daily transcriptional rhythms, male mice were maintained under standard 12h:12h light/dark conditions (LD), and four eight-week-old mice were collected per time point. To profile circadian transcription, seven-week-old female mice were maintained in constant darkness (DD) for between 156 and 176 hours and then sacrificed (at eight weeks of age); four mice were harvested per time point. We defined CT0 and 12 as the "lights on" (8am) and "lights off" (8pm) timings of the pre-DD light regime, respectively. Eight-week-old mice were used to ensure that the mice were within telogen phase when the epidermis was collected; any mouse in anagen phase was excluded.

Generation of RE/RE mice

To generate RE/RE mice, *Bmal1*-stopFL mice[6] were crossed with K14-Cre mice[50] and *Syt10*-Cre mice[21]. Female triple heterozygous mice (*Arntl*$^{stopFL/wt}$; K14-Cre$^{tg/wt}$;*Syt10*-Cre$^{tg/wt}$) were then crossed with male heterozygous *Bmal1*-stopFL mice (*Arntl*$^{stopFL/wt}$; K14-Cre$^{wt/wt}$;*Syt10*-Cre$^{wt/wt}$) to generate the five RE genotypes used in this manuscript: i) WT (WT), *Arntl*$^{wt/wt}$; K14-Cre$^{tg/wt}$;*Syt10*-Cre$^{tg/wt}$; ii) knockout (KO), *Arntl*$^{stopFL/stopFL}$; K14-Cre$^{wt/wt}$;*Syt10*-Cre$^{wt/wt}$; iii) epidermis-RE (epi-RE), *Arntl*$^{stopFL/stopFL}$; K14-Cre$^{tg/wt}$;*Syt10*-Cre$^{wt/wt}$; iv) brain-RE: *Arntl*$^{stopFL/stopFL}$; K14-Cre$^{wt/wt}$;*Syt10*-Cre$^{tg/wt}$; and v) double reconstituted (RE/RE): *Arntl*$^{stopFL/stopFL}$; K14-Cre$^{tg/wt}$;*Syt10*-Cre$^{tg/wt}$. All initial and maintenance crosses were performed using mice heterozygous for *Bmal1*-StopFL and each Cre, to avoid sterility associated with total *Bmal1* loss or unwanted transgene integration effects, respectively. Only female mice expressing the *Syt10*-Cre were used for breeding due to the known expression of this Cre in the testes of male mice that may lead to general recombination of the floxed loci[21].

METHOD DETAILS

Epidermis extraction

Mice were sacrificed by CO_2 asphyxiation, and death was confirmed by cervical dislocation. The mice were then shaved, and the back skin was subsequently removed and placed in ice-cold PBS. A tail sample was also taken to allow the genotype to be revalidated. To remove the hypodermis, the underside of the skin was then vigorously scraped using a scalpel. In a Petri dish, the skin was then floated on 10 ml of 1 mg/ml dispase (Sigma Aldrich) in PBS for 45 min at 37°C, to separate enzymatically the epidermis. Subsequently, using a scalpel, the epidermis was scraped from the surface of the skin and then mechanically disaggregated using surgical scissors. The disaggregated epidermis was then placed into 10 ml of ice-cold PBS + 10% chelated FBS to inactivate the dispase. After vigorous shaking, the epidermal extract was sequentially filtered through 100 µM and 40 µM filters to give a purified extract of epidermal cells. Cell viability was checked via Trypan blue staining, and pellets of one million cells were then lysed in 500 µl of TRIzol (Invitrogen) for subsequent RNA extraction.

Cell cycle analysis by flow cytometry

Epidermal cells were first extracted from 8-week-old male mice as described in 'Epidermis extraction' and then fixed in ice-cold 70% EtOH at -20°C for 2 hours. The cells were then washed 2x with PBS + 2% FBS + 1mM EDTA (wash buffer). The fixed cells were suspended to $1x10^7$cells/ml in wash buffer, and 100 µl of cell suspension was then mixed with 20 µl FITC anti-Ki67 antibody (BD Biosciences, 556026, AB_2649982) and incubated at room temperature for 20 min. The cells were then washed 1x with wash buffer and suspended in 500 µl wash buffer + 5 µg/ml propidium iodide. The proportion of actively cycling cells (Ki67-positive) in G1, S and G2 phase of the cell cycle (cell DNA content: 1n – G1, > 1n and < 2n – S, 2n – G2) was interrogated using a using a Gallios flow cytometer (Beckman Coulter) and subsequent data analysis with FlowJo (v.10.8.0). Quantification was performed using a minimum of 10,000 cells/sample.

EdU tracing of active epidermal DNA replication

WT or brain-RE mice (8-week-old males) were injected at ZT7 or ZT19 with 30mg/kg of EdU resuspended in PBS. After two hours, mice were sacrificed and $1cm^2$ pieces of back skin were fixed in 10% neutral buffered formalin (HT501128-4L, Sigma-Aldrich) at room temperature for 3 hours

and subsequently embedded in paraffin. To stain for EdU integration, 3-micron tissue sections were cut, deparaffinized and then stained using the Click-iT™ EdU Cell Proliferation Kit for Imaging (ThermoFisher, C10337) in accordance with the manufacturer's protocol. Sections were rinsed again with PBS and nuclei were counterstained with DAPI (1 μg ml–1) in PBS before mounting with Fluoromount (Sigma). The resulting slides were then scanned with a NanoZoomer 2.0HT (Hamamatsu) (40× objective at 0.46 μm/pixel). Representative images displayed in Figure S4B were produced using an a Zeiss LSM780 confocal microscope (63×/1.40 oil objective at 1024×1024 pixel resolution)

Ki67 histology staining

Full-thickness skin samples were fixed at RT for 3 hours with 10% neutral buffered formalin (HT501128-4L, Sigma-Aldrich). Paraffin-embedded tissue sections (2-3 μm) were air dried and further dried at 60 ºC over-night. Immunofluorescence for Anti Ki-67 (ab15580, abcam, AB_443209) was performed in a Leica Bond RX platform at 1:1000 for 120 min. Antigen retrieval was performed with BOND Epitope Retrieval 1 – ER1 (AR9961, Leica). Quenching of endogenous peroxidase was performed by 10 min of incubation with Peroxidase-Blocking Solution at RT (S2023, Dako, Agilent). Non-specific unions were blocked using 5 % of goat normal serum (16210064, Life technology) mixed with 2.5 % BSA diluted in wash buffer for 60 min at RT. Secondary antibody used was the Goat anti-Rabbit IgG H+L, Alexa Fluor 488 (A11034, ThermoFisher, AB_2576217) at 1:500 for 60 min. Nuclei were stained with DAPI (D9542, Sigma). Slides were mounted with the fluorescence Mounting Medium (S3023, Dako, Agilent). Specificity of staining was confirmed staining with the Rabbit IgG isotype control (NBP2-24891, Novus Biologicals). Fluorescent images were acquired with a NanoZoomer-2.0 HT C9600 digital scanner (Hamamatsu) equipped with a 20X objective and coupled to a mercury lamp unit L11600-05 and using NDP.scan3.4 software (Hamamatsu). All images were visualized with a gamma correction set at 1.0 in the image control panel of the NDP.view 2 U12388-01 software (Hamamatsu). DAPI signal of all the samples has been acquired with the filter DAPI350 with an exposure time of 56,96 ms and a gain of 4. Ki-67 Alexa Fluor 488 signal of all the samples has been acquired with the FITC filter with an exposure time of 113,93ms and a gain of 8.

RNA extraction

To extract total RNA, epidermal cells lysed in 500 μl TRIzol (Invitrogen) were vortexed with 100 μl chloroform, centrifuged for 15 min at 18,000 x *g* at 4°C, and then the upper aqueous layer containing

RNA was isolated. The aqueous layer was then mixed with 825 µl RLT buffer (Qiagen) and 625 µl 100% ethanol to induce RNA precipitation. Samples were then processed using an RNeasy mini kit (Qiagen) according to the manufacturer's protocol, and RNA was eluted in molecular biology–grade water and stored at –80°C.

RNA sequencing

Total RNA from mice was quantified by Qubit® RNA BR Assay kit (Thermo Fisher Scientific) and the RNA integrity was estimated by using RNA 6000 Nano Bioanalyzer 2100 Assay (Agilent). RNA-seq libraries were prepared with KAPA Stranded mRNA-Seq Illumina® Platforms Kit (Roche) following the manufacturer's recommendations. Briefly, following mRNA fragmentation, 500 ng of total RNA was used for the poly-A fraction enrichment with oligo-dT magnetic beads. Strand specificity was achieved for second-strand synthesis by using dUTP rather than dTTP. The blunt-ended, double-stranded cDNA was 3′-adenylated, and Illumina platform–compatible adaptors with unique dual indexes and unique molecular identifiers (Integrated DNA Technologies) were ligated onto them. The ligation product was enriched over 15 PCR cycles, and the final library was validated on an Agilent 2100 Bioanalyzer with the DNA 7500 assay. Libraries were sequenced using NovaSeq 6000 (Illumina) with a read length of 1x51bp+17bp+8bp, following the manufacturer's protocol. Image analysis, base calling, and quality scoring of the run were processed using the manufacturer's software Real Time Analysis (RTA 3.4.4).

Sequencing reads were first subjected to quality control and adapter trimming using Trimmomatic (version 0.36)[51]. Reads were then aligned to the mm10 genome (UCSC) using the HISAT2 aligner (version 2.2.1)[52] and subsequently sorted using SAMtools (version 1.3.1)[53]. After alignment, reads were quantified using featureCounts (version 1.6.0)[54], and the resulting count data was then normalized to generate RPKM values using the edgeR 'rpkm' function (version 3.18.1)[55].

QUANTIFICATION AND STATISTICAL ANALYSIS

Quantification of histology stainings

Quantification was performed using Qupath (v0.4.2) by manually selecting the epidermis, identifying DAPI positive regions and then calculating the percentage that were positive for EdU or Ki67 staining.

Identification of circadian genes and differential expression analysis

To generate consensus diurnal/circadian transcriptomes, the Jonckheere-Terpstra-Kendall (JTK_CYCLE)[29] and BIO_CYCLE[28] algorithms were used. In both instances, RPKM normalized gene expression values (log_2 transformed) were used as input. Genes were considered to be rhythmically expressed if they showed a period of 24 hours and *P*-value ≤ 0.01. The lists of genes found to be rhythmically expressed were then intersected, and those genes identified as rhythmic by both algorithms were defined as the consensus diurnal/circadian transcriptome.

To identify specific genes reliant upon different clock communication pathways for their rhythmic expression, the DryR algorithm[32] was applied to all datasets. Raw RNAseq counts were used as input, and the function 'dryseq()' was applied to run the algorithm. The resulting output was then filtered (BICW ≥ 0.4, Amp ≥ 0.25, Periodicity = 24 hours), to generate the gene sets then further analyzed.

To identify genes that were differentially expressed irrespective of time-of-day, we applied the 'deLimma' function within the LimoRhyde[56] workflow to compare our WT and RE/RE diurnal RNA-seq datasets. Differentially expressed genes were defined as those having a Padj ≤ 0.05 and fold-change ≥ 1.5.

All heat maps were generated using the pheatmap package in the R programming environment. For heat maps of the consensus diurnal/circadian transcriptomes, the mean of RPKM normalized gene expression values (log_2 transformed) from each time point were used as input to calculate a Z-score. For heat maps of the DryR-generated gene sets, the normalized read counts (as calculated by DryR) from each time point were used as input to calculate a Z-score. In all heat maps, genes were ordered by their calculated phase and a Z-score was calculated to visualize circadian expression patterns.

Amplitude and phase plots were generated using values calculated by the JTK_CYCLE algorithm or DryR (the algorithm used is stated in the associated figure legend), and all graphs were made using the ggplot2 package in the R programming environment. To calculate amplitude density, the 'geom_density' function from the ggplot2 package was used to calculate a smoothed density estimate of the amplitude values.

GO, Reactome, and motif analyses

All Gene Ontology (GO), Reactome and analyses of transcription factor targets were performed using the gene list enrichment analysis tool Enrichr[57]. GO and Reactome terms found to be enriched within the lists 'GO Biological Processes 2021' and 'Reactome 2022', respectively, were analyzed further. Enriched terms shown in the figures of this paper were manually filtered to remove redundant terms and to emphasize the enrichment of biologically important categories. To identify enrichment for known transcription factor targets, the dataset 'ENCODE and ChEA consensus TFs from ChIP-X' was used. The complete output from Enrichr for GO and Reactome can be found in Supplemental tables 1 and 2.

Statistics

JTK_Cycle was used to calculate the significance of gene expression or cell cycle rhythms when calculation of the significance of individual patterns was required. In all figures, ns, non-significant; $*P \leq 0.05$; $**P \leq 0.01$; $***P \leq 0.001$. All other information related to total number of replicates and other relevant statistical information is stated in the figure legends for all graphs.

Excel table titles and legends

Table S1. Specific gene sets generated by this study, related to Figures 1, 2, 3, 6, S1, S2, S3, S4, S6

Table S2, Gene Ontology and Reactome analyses generated by this study, related to Figures 1, 2, 3, 6, S1, S2, S3, S4, S6

References

1. López-Otín, C., and Kroemer, G. (2021). Hallmarks of Health. Preprint at Cell Press, 10.1016/j.cell.2020.11.034 10.1016/j.cell.2020.11.034.
2. Benitah, S.A., and Welz, P.S. (2020). Circadian Regulation of Adult Stem Cell Homeostasis and Aging. Cell Stem Cell *26*, 817–831. 10.1016/j.stem.2020.05.002.
3. Takahashi, J.S. (2017). Transcriptional architecture of the mammalian circadian clock. Nat Rev Genet *18*, 164–179. 10.1038/NRG.2016.150.
4. Hastings, M.H., Maywood, E.S., and Brancaccio, M. (2018). Generation of circadian rhythms in the suprachiasmatic nucleus. Nat Rev Neurosci *19*, 453–469. 10.1038/s41583-018-0026-z.

5. Husse, J., Leliavski, A., Tsang, A.H., Oster, H., and Eichele, G. (2014). The light-dark cycle controls peripheral rhythmicity in mice with a genetically ablated suprachiasmatic nucleus clock. FASEB Journal *28*, 4950–4960. 10.1096/fj.14-256594.

6. Welz, P.S., Zinna, V.M., Symeonidi, A., Koronowski, K.B., Kinouchi, K., Smith, J.G., Guillén, I.M., Castellanos, A., Crainiciuc, G., Prats, N., et al. (2019). BMAL1-Driven Tissue Clocks Respond Independently to Light to Maintain Homeostasis. Cell *177*, 1436-1447.e12. 10.1016/j.cell.2019.05.009.

7. Koronowski, K.B., Kinouchi, K., Welz, P.S., Smith, J.G., Zinna, V.M., Shi, J., Samad, M., Chen, S., Magnan, C.N., Kinchen, J.M., et al. (2019). Defining the Independence of the Liver Circadian Clock. Cell *177*, 1448-1462.e14. 10.1016/j.cell.2019.04.025.

8. Smith, J.G., Koronowski, K.B., Mortimer, T., Sato, T., Greco, C.M., Petrus, P., Verlande, A., Chen, S., Samad, M., Deyneka, E., et al. (2023). Liver and muscle circadian clocks cooperate to support glucose tolerance in mice. Cell Rep *42*. 10.1016/J.CELREP.2023.112588.

9. Dyar, K.A., Lutter, D., Artati, A., Ceglia, N.J., Liu, Y., Armenta, D., Jastroch, M., Schneider, S., de Mateo, S., Cervantes, M., et al. (2018). Atlas of Circadian Metabolism Reveals System-wide Coordination and Communication between Clocks. Cell *174*, 1571-1585.e11. 10.1016/j.cell.2018.08.042.

10. Guan, D., Xiong, Y., Trinh, T.M., Xiao, Y., Hu, W., Jiang, C., Dierickx, P., Jang, C., Rabinowitz, J.D., and Lazar, M.A. (2020). The hepatocyte clock and feeding control chronophysiology of multiple liver cell types. Science (1979) *369*, 1388–1395. 10.1126/SCIENCE.ABA8984.

11. Greco, C.M., Koronowski, K.B., Smith, J.G., Shi, J., Kunderfranco, P., Carriero, R., Chen, S., Samad, M., Welz, P.S., Zinna, V.M., et al. (2021). Integration of feeding behavior by the liver circadian clock reveals network dependency of metabolic rhythms. Sci Adv. 10.1126/sciadv.abi7828.

12. Manella, G., Sabath, E., Aviram, R., Dandavate, V., Ezagouri, S., Golik, M., Adamovich, Y., and Asher, G. (2021). The liver-clock coordinates rhythmicity of peripheral tissues in response to feeding. Nat Metab. 10.1038/s42255-021-00395-7.

13. de Assis, L.V.M., and Oster, H. (2021). The circadian clock and metabolic homeostasis: entangled networks. Preprint at Springer Science and Business Media Deutschland GmbH, 10.1007/s00018-021-03800-2 10.1007/s00018-021-03800-2.

14. Masri, S., Papagiannakopoulos, T., Kinouchi, K., Liu, Y., Cervantes, M., Baldi, P., Jacks, T., and Sassone-Corsi, P. (2016). Lung Adenocarcinoma Distally Rewires Hepatic Circadian Homeostasis. Cell *165*, 896–909. 10.1016/j.cell.2016.04.039.

15. Sato, S., Solanas, G., Peixoto, F.O., Bee, L., Symeonidi, A., Schmidt, M.S., Brenner, C., Masri, S., Benitah, S.A., and Sassone-Corsi, P. (2017). Circadian Reprogramming in the Liver Identifies Metabolic Pathways of Aging. Cell *170*, 664-677.e11. 10.1016/j.cell.2017.07.042.

16. Schaum, N., Lehallier, B., Hahn, O., Pálovics, R., Hosseinzadeh, S., Lee, S.E., Sit, R., Lee, D.P., Losada, P.M., Zardeneta, M.E., et al. (2020). Ageing hallmarks exhibit organ-specific temporal signatures. Nature. 10.1038/s41586-020-2499-y.

17. Stringari, C., Wang, H., Geyfman, M., Crosignani, V., Kumar, V., Takahashi, J.S., Andersen, B., and Gratton, E. (2015). In Vivo Single-Cell Detection of Metabolic Oscillations in Stem Cells. Cell Rep. 10.1016/j.celrep.2014.12.007.

18. Geyfman, M., Kumar, V., Liu, Q., Ruiz, R., Gordon, W., Espitia, F., Cam, E., Millar, S.E., Smyth, P., Ihler, A., et al. (2012). Brain and muscle Arnt-like protein-1 (BMAL1) controls circadian cell proliferation and susceptibility to UVB-induced DNA damage in the epidermis. Proc Natl Acad Sci U S A *109*, 11758–11763. 10.1073/pnas.1209592109.

19. Solanas, G., Peixoto, F.O., Perdiguero, E., Jardí, M., Ruiz-Bonilla, V., Datta, D., Symeonidi, A., Castellanos, A., Welz, P.S., Caballero, J.M., et al. (2017). Aged Stem Cells Reprogram Their Daily Rhythmic Functions to Adapt to Stress. Cell. 10.1016/j.cell.2017.07.035.

20. Janich, P., Toufighi, K., Solanas, G., Luis, N.M., Minkwitz, S., Serrano, L., Lehner, B., and Benitah, S.A. (2013). Human epidermal stem cell function is regulated by circadian oscillations. Cell Stem Cell. 10.1016/j.stem.2013.09.004.

21. Husse, J., Zhou, X., Shostak, A., Oster, H., and Eichele, G. (2011). Synaptotagmin10-cre, a driver to disrupt clock genes in the SCN. J Biol Rhythms *26*, 379–389. 10.1177/0748730411415363.

22. Petrus, P., Smith, J.G., Koronowski, K.B., Chen, S., Sato, T., Greco, C.M., Mortimer, T., Welz, P.-S., Zinna, V.M., Shimaji, K., et al. (2022). The central clock suffices to drive the majority of circulatory metabolic rhythms. Sci Adv *8*, eabo2896. 10.1126/sciadv.abo2896.

23. Tanioka, M., Yamada, H., Doi, M., Bando, H., Yamaguchi, Y., Nishigori, C., and Okamura, H. (2009). Molecular clocks in mouse skin. Journal of Investigative Dermatology. 10.1038/jid.2008.345.

24. Fonjallaz, P., Ossipow, V., Wanner, G., and Schibler, U. (1996). The two PAR leucine zipper proteins, TEF and DBP, display similar circadian and tissue-specific expression, but have different target promoter preferences. EMBO Journal. 10.1002/j.1460-2075.1996.tb00365.x.

25. Gachon, F., Fonjallaz, P., Damiola, F., Gos, P., Kodama, T., Zakany, J., Duboule, D., Petit, B., Tafti, M., and Schibler, U. (2004). The loss of circadian PAR bZip transcription factors results in epilepsy. Genes Dev *18*, 1397. 10.1101/GAD.301404.

26. Ripperger, J.A., Shearman, L.P., Reppert, S.M., and Schibler, U. (2000). CLOCK, an essential pacemaker component, controls expression of the circadian transcription factor DBP. Genes Dev. 10.1101/gad.14.6.679.

27. Wu, G., Ruben, M.D., Francey, L.J., Lee, Y.Y., Anafi, R.C., and Hogenesch, J.B. (2022). An in silico genome-wide screen for circadian clock strength in human samples. Bioinformatics *38*, 5375–5382. 10.1093/bioinformatics/btac686.

28. Agostinelli, F., Ceglia, N., Shahbaba, B., Sassone-Corsi, P., and Baldi, P. (2016). What time is it? Deep learning approaches for circadian rhythms. Bioinformatics *32*, i8–i17. 10.1093/bioinformatics/btw243.

29. Hughes, M.E., Hogenesch, J.B., and Kornacker, K. (2010). JTK_CYCLE: an efficient nonparametric algorithm for detecting rhythmic components in genome-scale data sets. J Biol Rhythms *25*, 372–380. 10.1177/0748730410379711.

30. Hughes, M.E., Abruzzi, K.C., Allada, R., Anafi, R., Arpat, A.B., Asher, G., Baldi, P., de Bekker, C., Bell-Pedersen, D., Blau, J., et al. (2017). Guidelines for Genome-Scale Analysis of Biological Rhythms. J Biol Rhythms *32*, 380–393. 10.1177/0748730417728663.

31. Pelikan, A., Herzel, H., Kramer, A., and Ananthasubramaniam, B. (2022). Venn diagram analysis overestimates the extent of circadian rhythm reprogramming. FEBS J *289*, 6605–6621. 10.1111/febs.16095.

32. Weger, B.D., Gobet, C., David, F.P.A., Atger, F., Martin, E., Phillips, N.E., Charpagne, A., Weger, M., Naef, F., and Gachon, F. (2021). Systematic analysis of differential rhythmic liver gene expression mediated by the circadian clock and feeding rhythms. Proc Natl Acad Sci U S A *118*. 10.1073/PNAS.2015803118.

33. Liao, G.-B., Li, X.-Z., Zeng, S., Liu, C., Yang, S.-M., Yang, L., Hu, C.-J., and Bai, J.-Y. (2018). Regulation of the master regulator FOXM1 in cancer. Cell Commun Signal *16*, 57. 10.1186/s12964-018-0266-6.

34. Petrenko, V., Stolovich-Rain, M., Vandereycken, B., Giovannoni, L., Storch, K.-F., Dor, Y., Chera, S., and Dibner, C. (2020). The core clock transcription factor BMAL1 drives circadian β-cell proliferation during compensatory regeneration of the endocrine pancreas. Genes Dev *34*, 1650–1665. 10.1101/gad.343137.120.

35. Farshadi, E., Yan, J., Leclere, P., Goldbeter, A., Chaves, I., and van der Horst, G.T.J. (2019). The positive circadian regulators CLOCK and BMAL1 control G2/M cell cycle transition through Cyclin B1. Cell Cycle *18*, 16–33. 10.1080/15384101.2018.1558638.

36. Breitkreutz, D., Koxholt, I., Thiemann, K., and Nischt, R. (2013). Skin basement membrane: the foundation of epidermal integrity--BM functions and diverse roles of bridging molecules nidogen and perlecan. Biomed Res Int *2013*, 179784. 10.1155/2013/179784.

37. Watt, F.M., Frye, M., and Benitah, S.A. (2008). MYC in mammalian epidermis: how can an oncogene stimulate differentiation? Preprint, 10.1038/nrc2328 10.1038/nrc2328.

38. Gaddameedhi, S., Selby, C.P., Kaufmann, W.K., Smart, R.C., and Sancar, A. (2011). Control of skin cancer by the circadian rhythm. Proc Natl Acad Sci U S A *108*, 18790–18795. 10.1073/pnas.1115249108.

39. Pickel, L., and Sung, H.-K. (2020). Feeding Rhythms and the Circadian Regulation of Metabolism. Front Nutr *7*, 39. 10.3389/fnut.2020.00039.

40. Damiola, F., le Minh, N., Preitner, N., Kornmann, B., Fleury-Olela, F., and Schibler, U. (2000). Restricted feeding uncouples circadian oscillators in peripheral tissues from the central pacemaker in the suprachiasmatic nucleus. Genes Dev *14*, 2950–2961. 10.1101/gad.183500.

41. Diamantopoulou, Z., Castro-Giner, F., Schwab, F.D., Foerster, C., Saini, M., Budinjas, S., Strittmatter, K., Krol, I., Seifert, B., Heinzelmann-Schwarz, V., et al. (2022). The metastatic spread of breast cancer accelerates during sleep. Nature *607*, 156–162. 10.1038/s41586-022-04875-y.

42. Kalucka, J., Missiaen, R., Georgiadou, M., Schoors, S., Lange, C., de Bock, K., Dewerchin, M., and Carmeliet, P. (2015). Metabolic control of the cell cycle. Cell Cycle *14*, 3379–3388. 10.1080/15384101.2015.1090068.

43. Janich, P., Pascual, G., Merlos-Suárez, A., Batlle, E., Ripperger, J., Albrecht, U., Cheng, H.Y.M., Obrietan, K., Di Croce, L., and Benitah, S.A. (2011). The circadian molecular clock creates epidermal stem cell heterogeneity. Nature. 10.1038/nature10649.

44. Buijs, R.M., Guzmán Ruiz, M.A., Méndez Hernández, R., and Rodríguez Cortés, B. (2019). The suprachiasmatic nucleus; a responsive clock regulating homeostasis by daily changing the setpoints of physiological parameters. Preprint at Elsevier B.V., 10.1016/j.autneu.2019.02.001 10.1016/j.autneu.2019.02.001.

45. Lunt, S.Y., and vander Heiden, M.G. (2011). Aerobic glycolysis: Meeting the metabolic requirements of cell proliferation. Annu Rev Cell Dev Biol *27*. 10.1146/annurev-cellbio-092910-154237.

46. Castillo-Armengol, J., Fajas, L., and Lopez-Mejia, I.C. (2019). Inter-organ communication: a gatekeeper for metabolic health. EMBO Rep *20*, e47903. 10.15252/embr.201947903.

47. Koronowski, K.B., and Sassone-Corsi, P. (2021). Communicating clocks shape circadian homeostasis. Science (1979) *371*. 10.1126/science.abd0951.

48. Shostak, A. (2017). Circadian Clock, Cell Division, and Cancer: From Molecules to Organism. Int J Mol Sci *18*. 10.3390/IJMS18040873.

49. Percie du Sert, N., Hurst, V., Ahluwalia, A., Alam, S., Avey, M.T., Baker, M., Browne, W.J., Clark, A., Cuthill, I.C., Dirnagl, U., et al. (2020). The ARRIVE guidelines 2.0: Updated guidelines for reporting animal research*. Journal of Cerebral Blood Flow and Metabolism *40*, 1769–1777. 10.1177/0271678X20943823.

50. Dassule, H.R., Lewis, P., Bei, M., Maas, R., and McMahon, A.P. (2000). Sonic hedgehog regulates growth and morphogenesis of the tooth. Development. 10.1242/dev.127.22.4775.

51. Bolger, A.M., Lohse, M., and Usadel, B. (2014). Trimmomatic: A flexible trimmer for Illumina sequence data. Bioinformatics. 10.1093/bioinformatics/btu170.

52. Kim, D., Paggi, J.M., Park, C., Bennett, C., and Salzberg, S.L. (2019). Graph-based genome alignment and genotyping with HISAT2 and HISAT-genotype. Nat Biotechnol. 10.1038/s41587-019-0201-4.

53. Li, H., Handsaker, B., Wysoker, A., Fennell, T., Ruan, J., Homer, N., Marth, G., Abecasis, G., Durbin, R., and 1000 Genome Project Data Processing Subgroup, 1000 Genome Project Data Processing (2009). The Sequence Alignment/Map format and SAMtools. Bioinformatics *25*, 2078–2079. 10.1093/bioinformatics/btp352.

54. Liao, Y., Smyth, G.K., and Shi, W. (2014). FeatureCounts: An efficient general purpose program for assigning sequence reads to genomic features. Bioinformatics. 10.1093/bioinformatics/btt656.

55. Robinson, M.D., McCarthy, D.J., and Smyth, G.K. (2010). edgeR: a Bioconductor package for differential expression analysis of digital gene expression data. Bioinformatics *26*, 139. 10.1093/BIOINFORMATICS/BTP616.

56. Singer, J.M., and Hughey, J.J. (2019). LimoRhyde: A Flexible Approach for Differential Analysis of Rhythmic Transcriptome Data. J Biol Rhythms *34*, 5–18. 10.1177/0748730418813785.

57. Chen, E.Y., Tan, C.M., Kou, Y., Duan, Q., Wang, Z., Meirelles, G. v., Clark, N.R., and Ma'ayan, A. (2013). Enrichr: Interactive and collaborative HTML5 gene list enrichment analysis tool. BMC Bioinformatics. 10.1186/1471-2105-14-128.

KEY RESOURCES TABLE

REAGENT or RESOURCE	SOURCE	IDENTIFIER	RRID
Antibodies			
anti-Ki67 (FACS)	BD Biosciences	Cat#556026	AB_2649982
anti-Ki67 (histology)	Abcam	Cat#ab15580	AB_443209
Goat anti-Rabbit IgG H+L, Alexa Fluor 488	Thermo Fisher Scientific	Cat#A11034	AB_2576217
Critical Commercial Assays			
Click-iT™ EdU Cell Proliferation Kit for Imaging	Thermo Fisher Scientific	Cat#C10337	N/A
RNeasy mini kit	Qiagen	Cat#74104	N/A
Deposited Data			
Circadian/diurnal RNA-seq data	this study	GSE190035	N/A
Experimental Models: Organisms/Strains			
Mouse: *Bmal1* Brain and Epidermis-Reconstituted – *Bmal1*$^{stopFL/stopFL}$; *K14*-cre$^{tg/wt}$; Syt10-cre$^{tg/wt}$	this study	N/A	N/A
Mouse: *Bmal1* Brain-Reconstituted – *Bmal1*$^{stopFL/stopFL}$; *K14*-cre$^{wt/wt}$; Syt10-cre$^{tg/wt}$	this study	N/A	N/A
Mouse: *Bmal1* Epidermis -Reconstituted – *Bmal1*$^{stopFL/stopFL}$; *K14*-cre$^{tg/wt}$; Syt10-cre$^{wt/wt}$	this study	N/A	N/A
Mouse: *Wild type - Bmal1*$^{wt/wt}$; *K14*-cre$^{tg/wt}$; Syt10-cretg/^{wt}	this study	N/A	N/A
Mouse: *Bmal1* Epidermis-specific knock-out - Bmal1$^{LoxP/LoxP}$;*K14*-cre$^{tg/wt}$	43	N/A	N/A
Mouse: *Bmal1* knockout – *Bmal1*$^{stopFL/stopFL}$	6	N/A	N/A
Mouse: Synaptotagmin 10 Cre - *Syt10*^{Cre}	21	N/A	N/A
Software and Algorithms			
Jonckheere-Terpstra-Kendall (JTK_CYCLE) algorithm	29	N/A	N/A
BIO_CYCLE algorithm	28	N/A	N/A
DryR algorithm	32	N/A	N/A
Prism 10.10	GraphPad	N/A	N/A
Trimmomatic (version 0.36)	51	N/A	N/A
HISAT2 (version 2.2.1)	52	N/A	N/A
SAMtools (version 1.3.1)	53	N/A	N/A
featureCounts (version 1.6.0)	54	N/A	N/A
edgeR (version 3.18.1)	55	N/A	N/A
LimoRhyde	56	N/A	N/A
QuPath (version 0.4.2)	QuPath	N/A	N/A

Figure 1

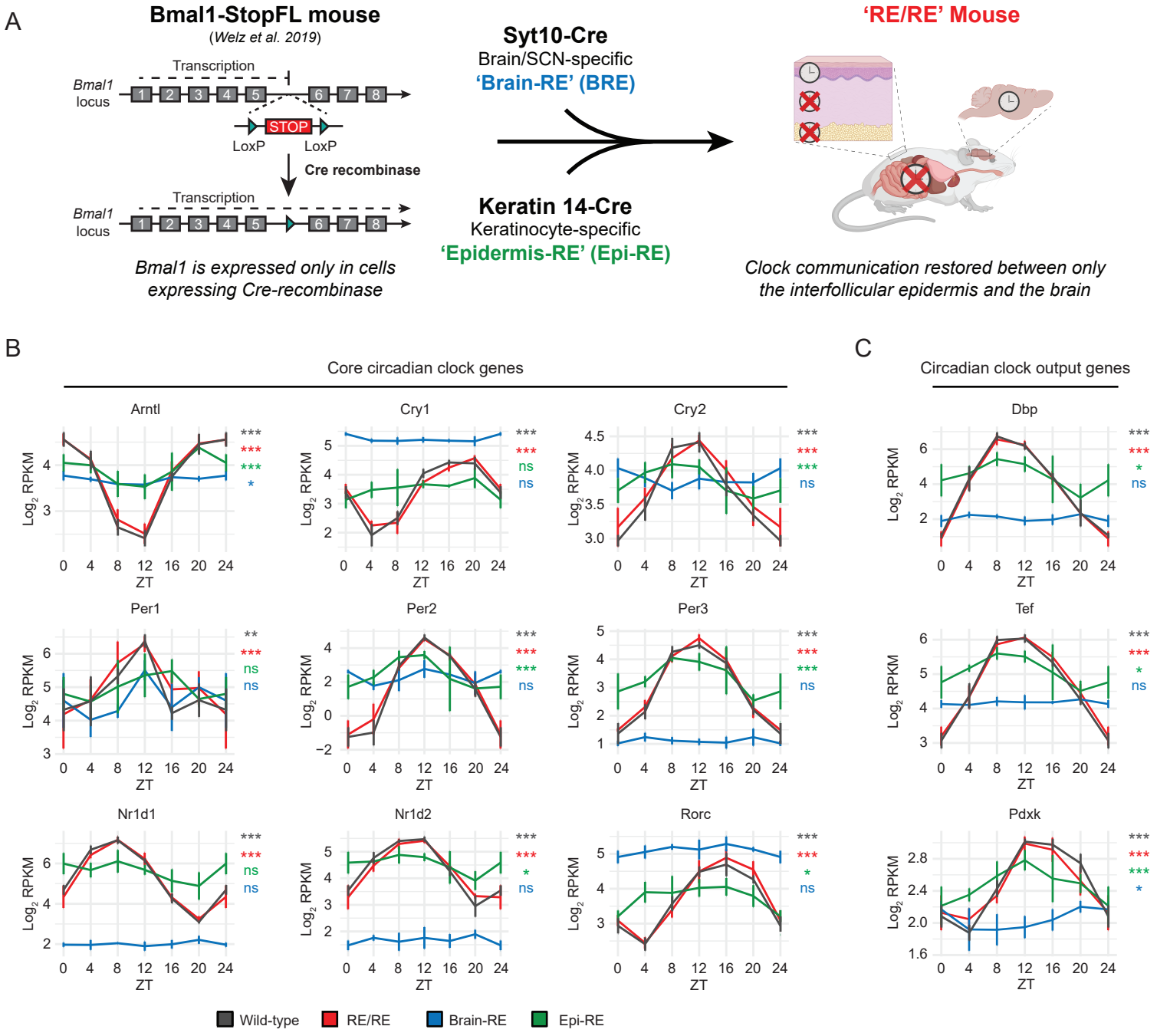
A
Bmal1-StopFL mouse
(Welz et al. 2019)
Transcription
Bmal1 locus
1 2 3 4 5 6 7 8
STOP
LoxP LoxP
Cre recombinase
Transcription
Bmal1 locus
1 2 3 4 5 6 7 8
Bmal1 is expressed only in cells expressing Cre-recombinase
Syt10-Cre
Brain/SCN-specific
'Brain-RE' (BRE)
Keratin 14-Cre
Keratinocyte-specific
'Epidermis-RE' (Epi-RE)
'RE/RE' Mouse
Clock communication restored between only the interfollicular epidermis and the brain
B
Core circadian clock genes
Arntl
Cry1
Cry2
Per1
Per2
Per3
Nr1d1
Nr1d2
Rorc
C
Circadian clock output genes
Dbp
Tef
Pdxk
Log2 RPKM
ZT
Wild-type
RE/RE
Brain-RE
Epi-RE
D
Consensus Diurnal Transcriptome
Rhythmically expressed genes
2046
1093
900
343
Wild-type RE/RE Brain-RE Epi-RE
E
Early cell cycle
G1/S transition of mitotic cell cycle
DNA replication initiation
DNA replication
Late cell cycle
Regulation of G2/M transition
Metaphase plate congression
Regulation of meta/ anaphase transition
Adj P-value (-Log10)
F
Aerobic electron transport chain
Mitochondrion organization
rRNA processing
Transcription by RNA polymerase II
Ubiquitin-dependent protein catabolic process
Retrograde vesicle-mediated transport, Golgi to ER
Ribosome biogenesis
Adj P-value (-Log10)

Figure 2

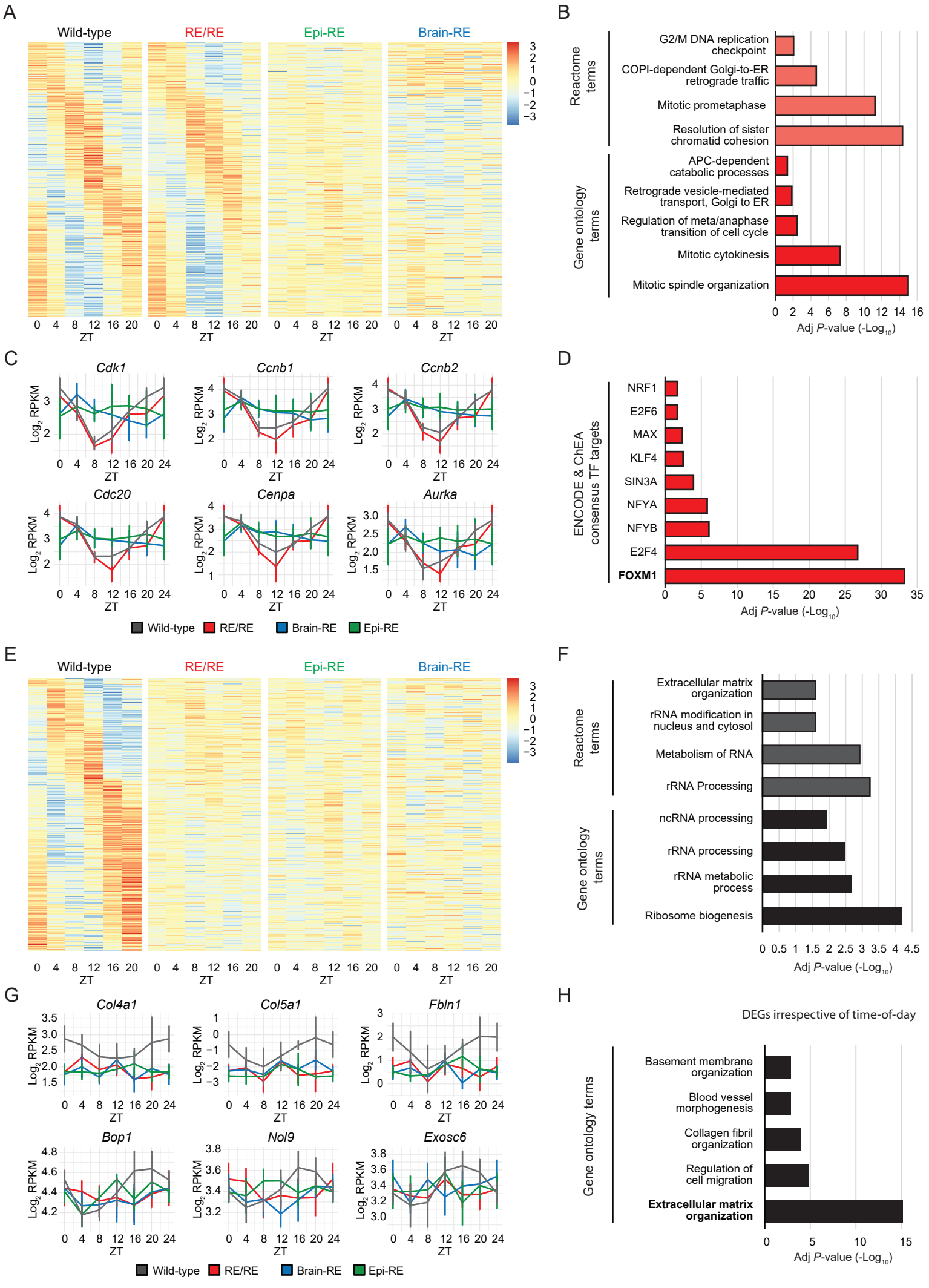
A
Wild-type
RE/RE
Epi-RE
Brain-RE
ZT
B
Reactome terms
G2/M DNA replication checkpoint
COPI-dependent Golgi-to-ER retrograde traffic
Mitotic prometaphase
Resolution of sister chromatid cohesion
Gene ontology terms
APC-dependent catabolic processes
Retrograde vesicle-mediated transport, Golgi to ER
Regulation of meta/anaphase transition of cell cycle
Mitotic cytokinesis
Mitotic spindle organization
Adj P-value (-Log10)
C
Cdk1
Ccnb1
Ccnb2
Cdc20
Cenpa
Aurka
Log2 RPKM
ZT
Wild-type
RE/RE
Brain-RE
Epi-RE
D
ENCODE & ChEA consensus TF targets
NRF1
E2F6
MAX
KLF4
SIN3A
NFYA
NFYB
E2F4
FOXM1
Adj P-value (-Log10)
E
Wild-type
RE/RE
Epi-RE
Brain-RE
ZT
F
Reactome terms
Extracellular matrix organization
rRNA modification in nucleus and cytosol
Metabolism of RNA
rRNA Processing
Gene ontology terms
ncRNA processing
rRNA processing
rRNA metabolic process
Ribosome biogenesis
Adj P-value (-Log10)
G
Col4a1
Col5a1
Fbln1
Bop1
Nol9
Exosc6
Log2 RPKM
ZT
Wild-type
RE/RE
Brain-RE
Epi-RE
H
DEGs irrespective of time-of-day
Gene ontology terms
Basement membrane organization
Blood vessel morphogenesis
Collagen fibril organization
Regulation of cell migration
Extracellular matrix organization
Adj P-value (-Log10)

Figure 3

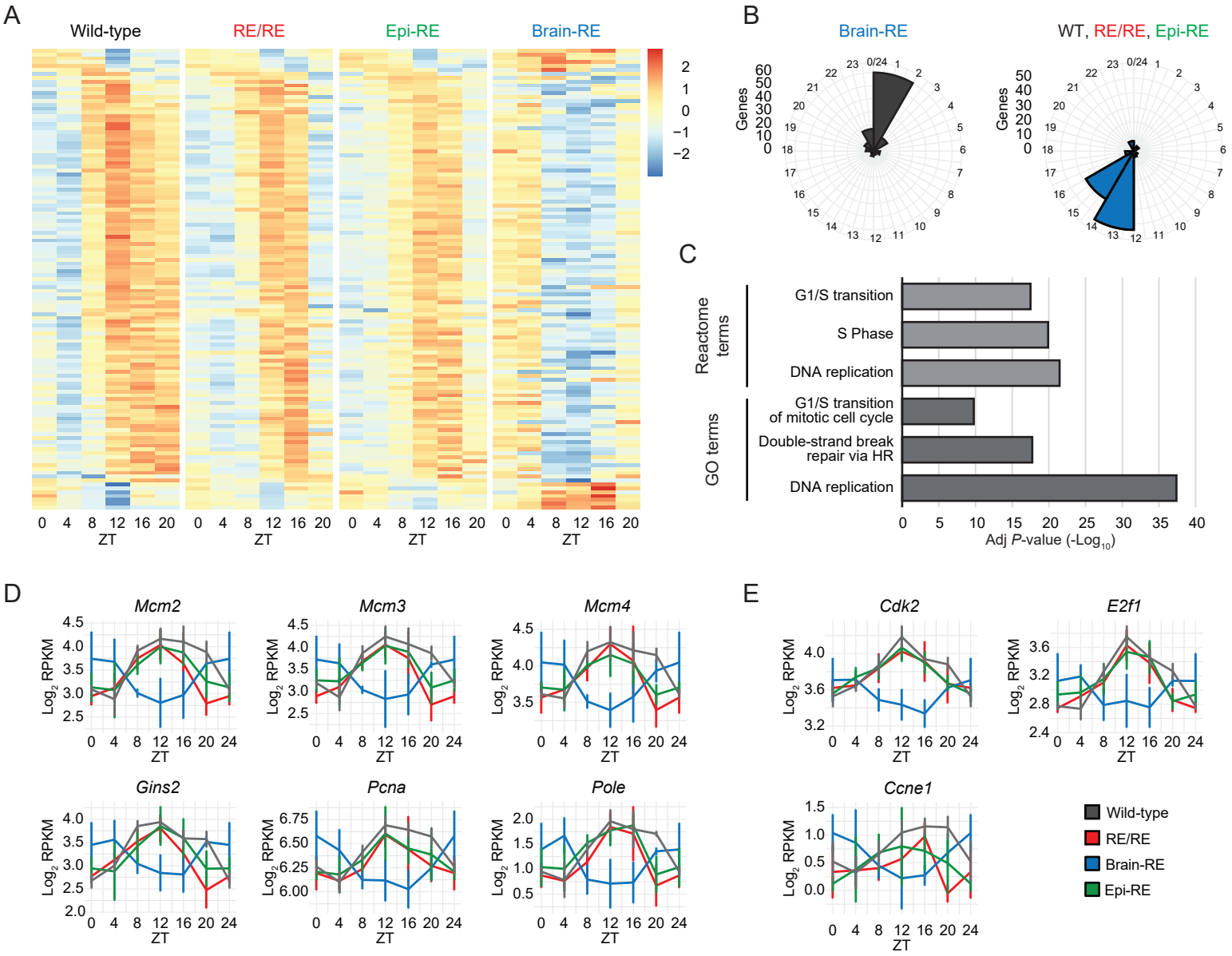
A
Wild-type
RE/RE
Epi-RE
Brain-RE
2
1
0
−1
−2
0 4 8 12 16 20
ZT
B
Brain-RE
WT, RE/RE, Epi-RE
Genes
C
Reactome terms
GO terms
G1/S transition
S Phase
DNA replication
G1/S transition of mitotic cell cycle
Double-strand break repair via HR
DNA replication
0 5 10 15 20 25 30 35 40
Adj P-value (-Log10)
D
Mcm2
Mcm3
Mcm4
Gins2
Pcna
Pole
Log2 RPKM
0 4 8 12 16 20 24
ZT
E
Cdk2
E2f1
Ccne1
Wild-type
RE/RE
Brain-RE
Epi-RE

Figure 4

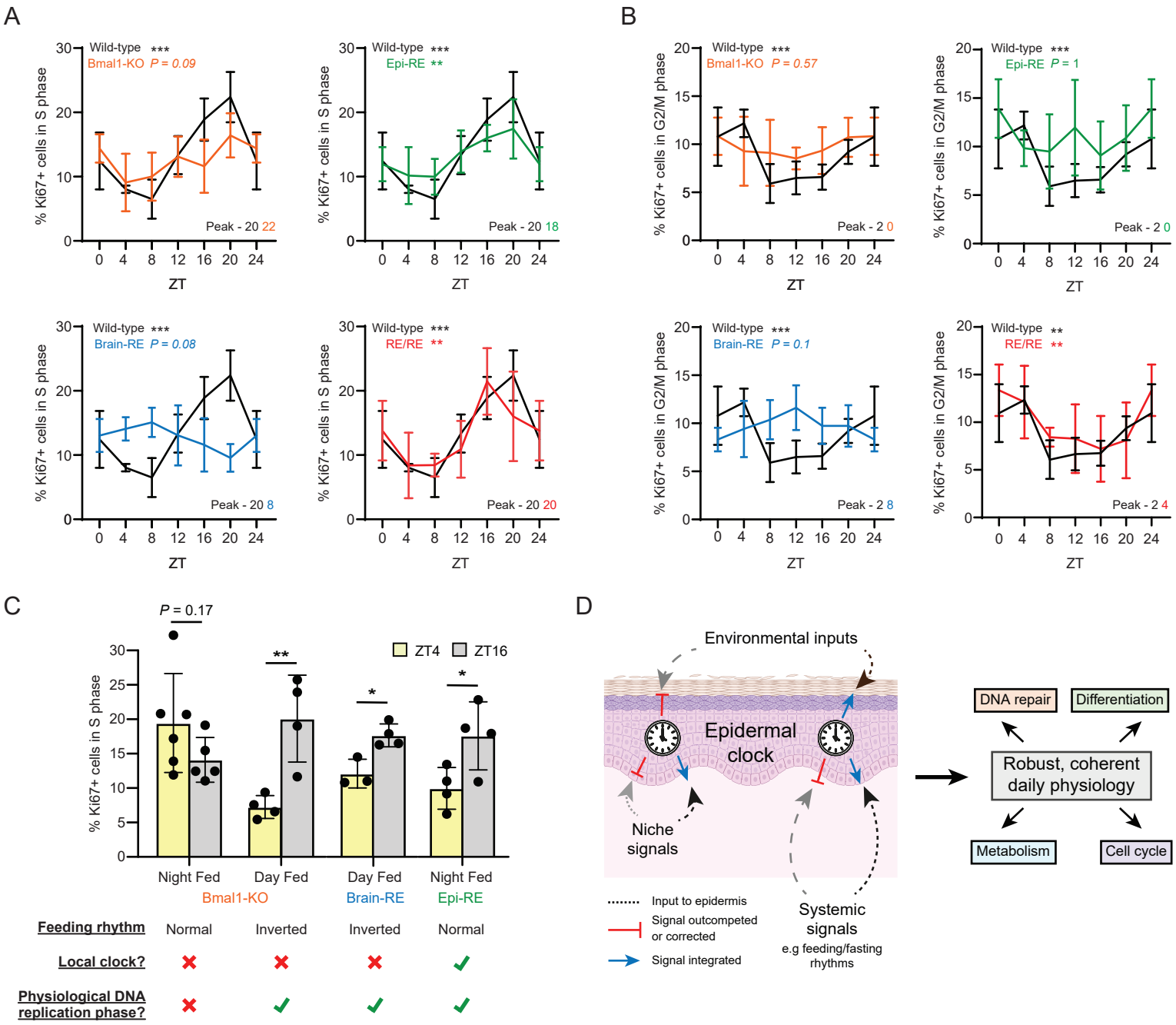
A
Wild-type ***
Bmal1-KO P = 0.09
Peak - 20 22
Wild-type ***
Epi-RE **
Peak - 20 18
Wild-type ***
Brain-RE P = 0.08
Peak - 20 8
Wild-type ***
RE/RE **
Peak - 20 20
% Ki67+ cells in S phase
ZT
B
Wild-type ***
Bmal1-KO P = 0.57
Peak - 2 0
Wild-type ***
Epi-RE P = 1
Peak - 2 0
Wild-type ***
Brain-RE P = 0.1
Peak - 2 8
Wild-type **
RE/RE **
Peak - 2 4
% Ki67+ cells in G2/M phase
ZT
C
P = 0.17
**
*
*
ZT4
ZT16
% Ki67+ cells in S phase
Night Fed
Day Fed
Day Fed
Night Fed
Bmal1-KO
Brain-RE
Epi-RE
Feeding rhythm
Normal
Inverted
Inverted
Normal
Local clock?
Physiological DNA replication phase?
D
Environmental inputs
Epidermal clock
Niche signals
Systemic signals
e.g feeding/fasting rhythms
Input to epidermis
Signal outcompeted or corrected
Signal integrated
DNA repair
Differentiation
Robust, coherent daily physiology
Metabolism
Cell cycle

Figure 5

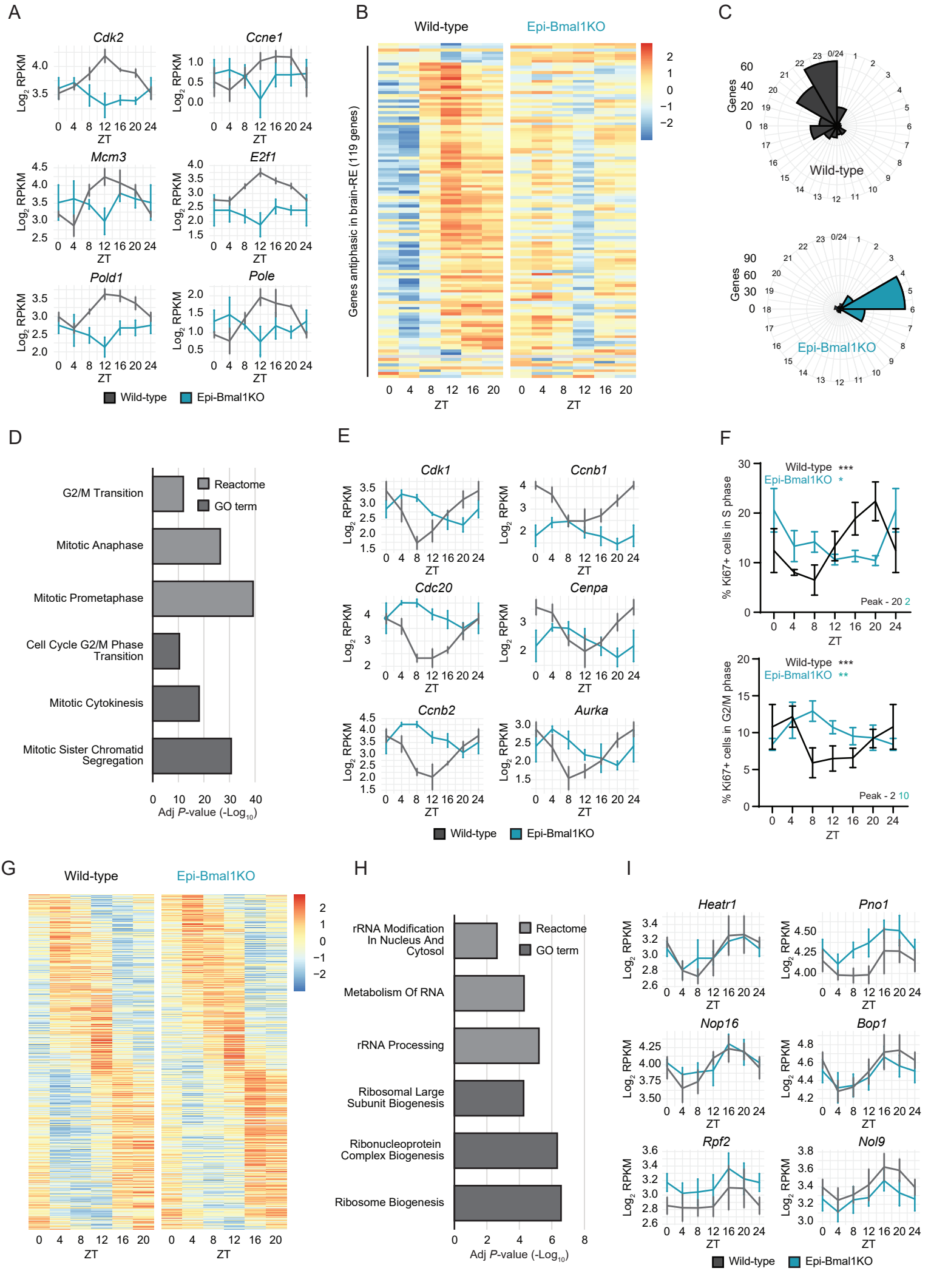
A
Cdk2
Ccne1
Mcm3
E2f1
Pold1
Pole
Log2 RPKM
ZT
Wild-type
Epi-Bmal1KO
B
Wild-type
Epi-Bmal1KO
Genes antiphasic in brain-RE (119 genes)
ZT
C
Genes
Wild-type
Epi-Bmal1KO
D
G2/M Transition
Mitotic Anaphase
Mitotic Prometaphase
Cell Cycle G2/M Phase Transition
Mitotic Cytokinesis
Mitotic Sister Chromatid Segregation
Reactome
GO term
Adj P-value (-Log10)
E
Cdk1
Ccnb1
Cdc20
Cenpa
Ccnb2
Aurka
Log2 RPKM
ZT
Wild-type
Epi-Bmal1KO
F
% Ki67+ cells in S phase
Wild-type ***
Epi-Bmal1KO *
Peak - 20 2
% Ki67+ cells in G2/M phase
Wild-type ***
Epi-Bmal1KO **
Peak - 2 10
ZT
G
Wild-type
Epi-Bmal1KO
ZT
H
rRNA Modification In Nucleus And Cytosol
Metabolism Of RNA
rRNA Processing
Ribosomal Large Subunit Biogenesis
Ribonucleoprotein Complex Biogenesis
Ribosome Biogenesis
Reactome
GO term
Adj P-value (-Log10)
I
Heatr1
Pno1
Nop16
Bop1
Rpf2
Nol9
Log2 RPKM
ZT
Wild-type
Epi-Bmal1KO

Figure 6

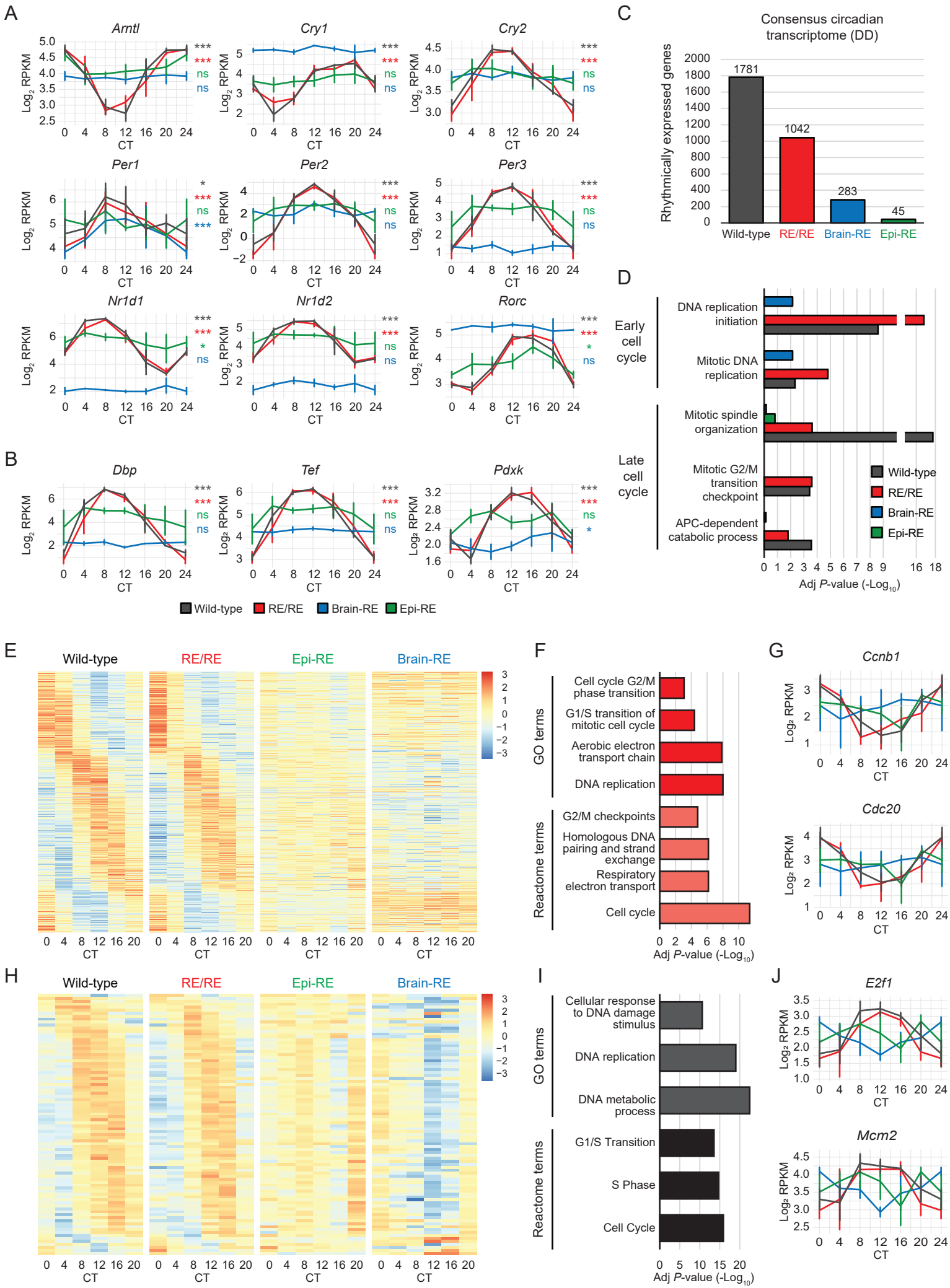
A
Arntl
Cry1
Cry2
Per1
Per2
Per3
Nr1d1
Nr1d2
Rorc
Log2 RPKM
CT
B
Dbp
Tef
Pdxk
Wild-type
RE/RE
Brain-RE
Epi-RE
C
Consensus circadian transcriptome (DD)
Rhythmically expressed genes
1781
1042
283
45
D
Early cell cycle
Late cell cycle
DNA replication initiation
Mitotic DNA replication
Mitotic spindle organization
Mitotic G2/M transition checkpoint
APC-dependent catabolic process
Adj P-value (-Log10)
E
F
GO terms
Reactome terms
Cell cycle G2/M phase transition
G1/S transition of mitotic cell cycle
Aerobic electron transport chain
DNA replication
G2/M checkpoints
Homologous DNA pairing and strand exchange
Respiratory electron transport
Cell cycle
G
Ccnb1
Cdc20
H
I
Cellular response to DNA damage stimulus
DNA metabolic process
G1/S Transition
S Phase
J
E2f1
Mcm2

Supplemental Items

Supplementary figure legends

Figure S1 - Communication with brain and other peripheral tissues ensures intact daily epidermal physiology, related to Figure 1, 2 and 3:

(A) Venn diagrams quantifying the intersect of diurnal transcriptomes identified using the JTK_CYCLE and BIO_CYCLE algorithms for all clock reconstitution conditions. (**B**) Heat map of the consensus diurnal transcriptomes (overlap of BIO_CYCLE and JTK_CYCLE-calculated diurnal transcriptomes) derived for each clock reconstitution condition (see A). (**C** and **D**) Circular histograms (C) and a density plot (D) indicating the distribution of expression phases and expression amplitudes (respectively) of genes constituting the epidermal diurnal transcriptome of each clock reconstitution condition. Both expression phases and expression amplitudes are those calculated by JTK_Cycle. (**E** and **G**) Circular histograms indicating the distribution of expression phases of genes equivalently rhythmic only in WT and RE/RE epidermis (629 genes) (E) or only rhythmic in WT epidermis (399 genes) (G). The phase values plotted correspond to those calculated by DryR for this model, and therefore the phases of all genes in (G) are considered equivalent for WT and RE/RE epidermis. (**F**) Diurnal expression pattern of *Foxm1* in the epidermis of each clock reconstitution condition (RNA-seq). Values represent the $\log_2$-transformed mean (± standard deviation) RPKM of $n = 4$ biological replicates. The time point ZT0 is double-plotted. (**H**) Enrichment of known transcription factor targets amongst genes rhythmic in WT epidermis only. **(I)** Pie chart indicating the number of the genes with antiphasic rhythmicity in brain-RE epidermis that also exhibited rhythmicity in the epidermis of *Bmal1*-StopFL mice (whole-body *Bmal1* null). Data for *Bmal1*-StopFL mice were sourced from Welz *et al*, (2019), and rhythmicity was defined as a JTK_CYCLE calculated periodicity of 24 hours and $P \leq 0.01$. ChEA, ChIP Enrichment Analysis; ENCODE, Encyclopedia of DNA Elements.

Figure S2 – Gene expression arrhythmicity does not originate from inter-individual phase dispersion, related to Figure 2

(A&B) Violin plot showing the distribution of gene expression standard deviations for all time points of genes rhythmic in WT+RE/RE epidermis only (629 genes - Figure 2A) (A) and WT+RE/RE+brain-RE epidermis only (608 genes). Lines represent median +/- interquartile range. To calculate

significance, a paired Student's t-test (A) or one-way ANOVA test (B) was performed. **C)** Violin plot showing the distribution of gene expression standard deviations for all time points of all genes in all conditions. Genes with a standard deviation of zero in any condition were excluded. Box plots represent median +/- interquartile range. Values > 0.5 are not displayed for visualisation purposes. To calculate significance, a one-way ANOVA test was performed. **D)** Violin plot showing the distribution of expression amplitudes for the consensus rhythmic transcriptomes of all conditions (Figure 1D). Box plots represent median +/- interquartile range. Values > 1 and < -5 are not displayed for visualisation purposes. To calculate significance, a one-way ANOVA test was performed. **E)** A dot plot comparing the gene expression amplitude of core clock genes in WT and RE/RE epidermis. Each dot represents one of the core clock genes displayed in Figure 1B. To calculate significance, an unpaired Student's t-test was performed. Md, mean difference vs WT.

Figure S3 – Expression magnitude classification of genes regulated by different clock communication pathways, related to Figure 2

(A, C, E and G) Heat maps showing the diurnal expression patterns of: (A) genes requiring brain:epidermal communication (WT+RE/RE only, 608 genes - Figure 2A) that also show equivalent mean expression in all conditions (211 genes); (C) Genes requiring brain:epidermal communication (WT+RE/RE only, 608 genes - Figure 2A) that show equivalent mean expression in WT, RE/RE and epi-RE, but decreased or increased expression in brain-RE (205 genes); (E) Genes requiring peripheral:epidermal clock communication (WT only, 389 genes – Figure 2E) that show equivalent mean expression in all conditions (166 genes); (G) Genes requiring peripheral:epidermal clock communication (WT only, 389 genes – Figure 2E) that show higher expression in WT relative to all other conditions (77 genes). Genes were categorized by their most probable 'mean model' as determined by DryR. Genes are sorted by expression phase. **(B, D, F and H)** Selected Gene Ontology and Reactome terms enriched amongst the gene classes presented in the heat map shown opposite.

Figure S4 - Brain clock signals drive an antiphasic pattern of epidermal DNA replication, related to Figure 4

(A) Percentage of epidermal cells positive for nuclear EdU staining after a two-hour day (ZT7-9) or night (ZT19-21) incubation period i.e. actively replicating their DNA during that period. Values represent the mean (± standard deviation) of $n = 3$ biological replicates. **(B)** Representative images of the experiment described in (A). Scale bars = 25 μm. (**C**) Percentage of epidermal cells actively

proliferating (Ki67-positive) across a 24-hour cycle as quantified by immunofluorescence staining of skin samples. Values represent the mean (± standard deviation) of n = 3-4 biological replicates. The *P* values displayed were calculated using JTK_Cycle. (**D**) Comparison of the total number of proliferating cells found in the epidermis of each model. All replicates of quantified Ki67 stainings shown in (C) were pooled to generate this comparison. To calculate significance, an unpaired Student's t-test was performed. ZT, *Zeitgeber* time.

Figure S5 - The epidermal clock gates extracellular signaling inputs in the physiological state, related to Figure 5:

(**A** and **B**) Circadian expression patterns of core clock genes (A) and clock-controlled genes (B) in the epidermis of wild-type and epi-Bmal1KO mice (RNA-seq). The time point ZT0 is double-plotted. Values represent the $\log_2$-transformed mean (± standard deviation) RPKM of $n = 4$ biological replicates. **(C** and **E)** Heat map showing the circadian expression patterns of genes rhythmic only in WT epidermis (323 genes) (C) or with phase shifted rhythmicity in epi-Bmal1KO relative to WT (234 genes) (E), in WT and epi-Bmal1KO conditions. Colors represent a Z-score calculated using the normalized read counts (as calculated by DryR) from each time point. Genes are sorted by expression phase. **(D)** Selected Gene Ontology and Reactome terms enriched amongst genes rhythmic in WT, but not epi-Bmal1KO epidermis. RPKM, reads per kilobase per million mapped reads; ZT, *Zeitgeber* time.

Figure S6 - Brain clock communication ensures robust daily epidermal physiology in constant darkness, related to Figure 6:

(**A**) A graphic depiction of how DD experiments were performed in this study. **(B)** Venn diagrams quantifying the intersect of circadian transcriptomes identified by the JTK_CYCLE and BIO_CYCLE algorithms for all clock reconstitution conditions. (**C**) Heat map of the consensus circadian transcriptomes (overlap of BIO_CYCLE and JTK_CYCLE-calculated circadian transcriptomes) derived for each clock reconstitution condition (see A). Colors represent a Z-score calculated using the mean RPKM from each time point. (**D** and **E**) Circular histograms (D) and a density plot (E) indicating the distribution of expression phases and expression amplitudes (respectively) of genes constituting the epidermal circadian transcriptome of each clock reconstitution condition. Both expression phases and expression amplitudes are those calculated by JTK_Cycle. (**F** and **H**) Circular histograms indicating the distribution of expression phases of genes equivalently rhythmic only in

WT and RE/RE epidermis (961 genes) (F) or with antiphasic rhythmicity in brain-RE epidermis relative to wild-type and RE/RE (89 genes) (H). The phase values plotted in correspond to those calculated by DryR for this model, and therefore in (H) the phase of all gene is considered equivalent in wild-type and RE/RE. (**G** and **I**) Circadian expression patterns of late (B) and early (D) cell cycle regulators in the epidermis of each clock reconstitution condition, as determined by RNA-seq. Values represent the $\log_2$-transformed mean (± standard deviation) RPKM of $n = 4$ biological replicates. The time point CT0 is double-plotted for better visualization. CT, circadian time.

Supplementary Figure 1

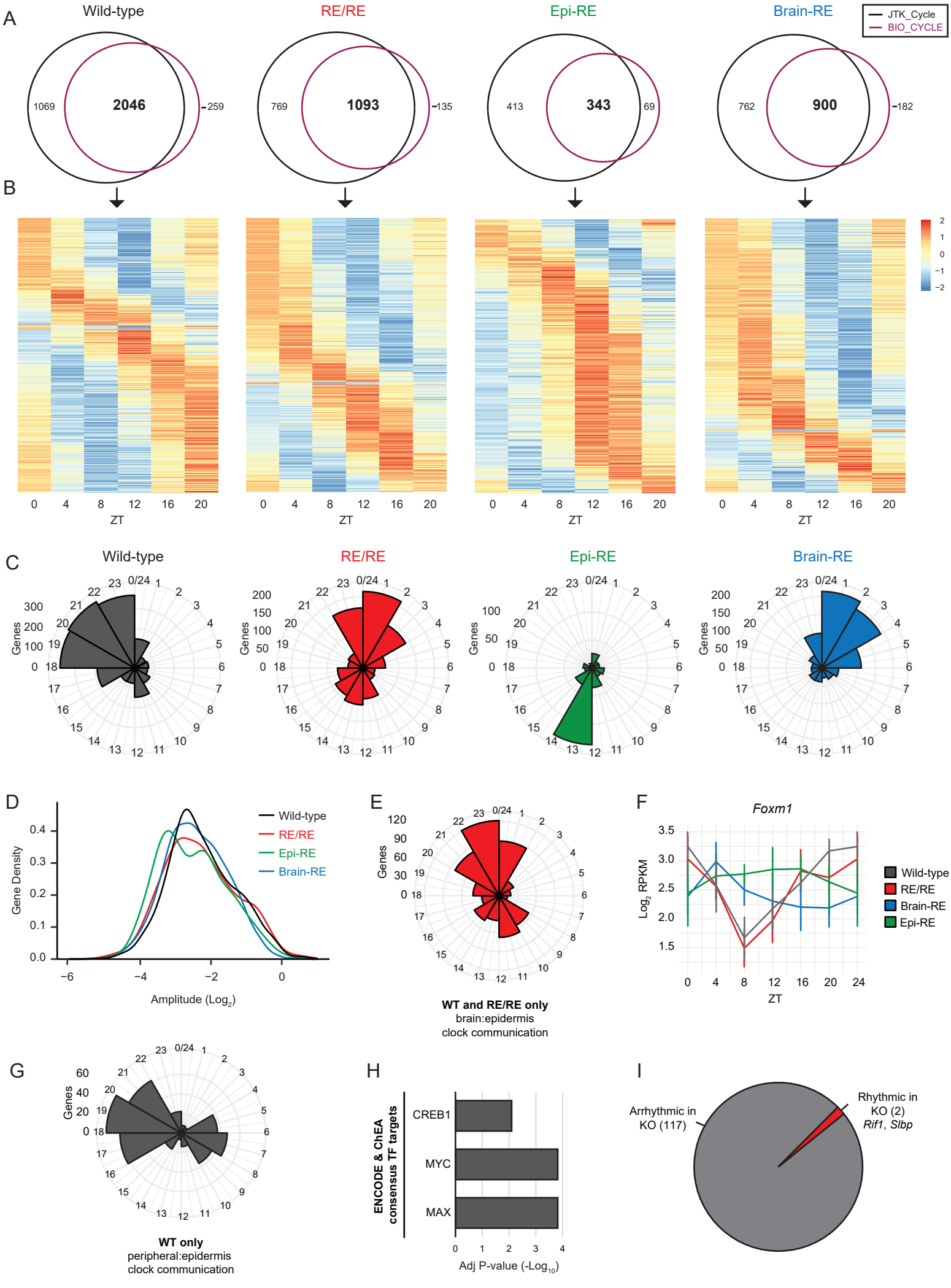

Supplementary Figure 2

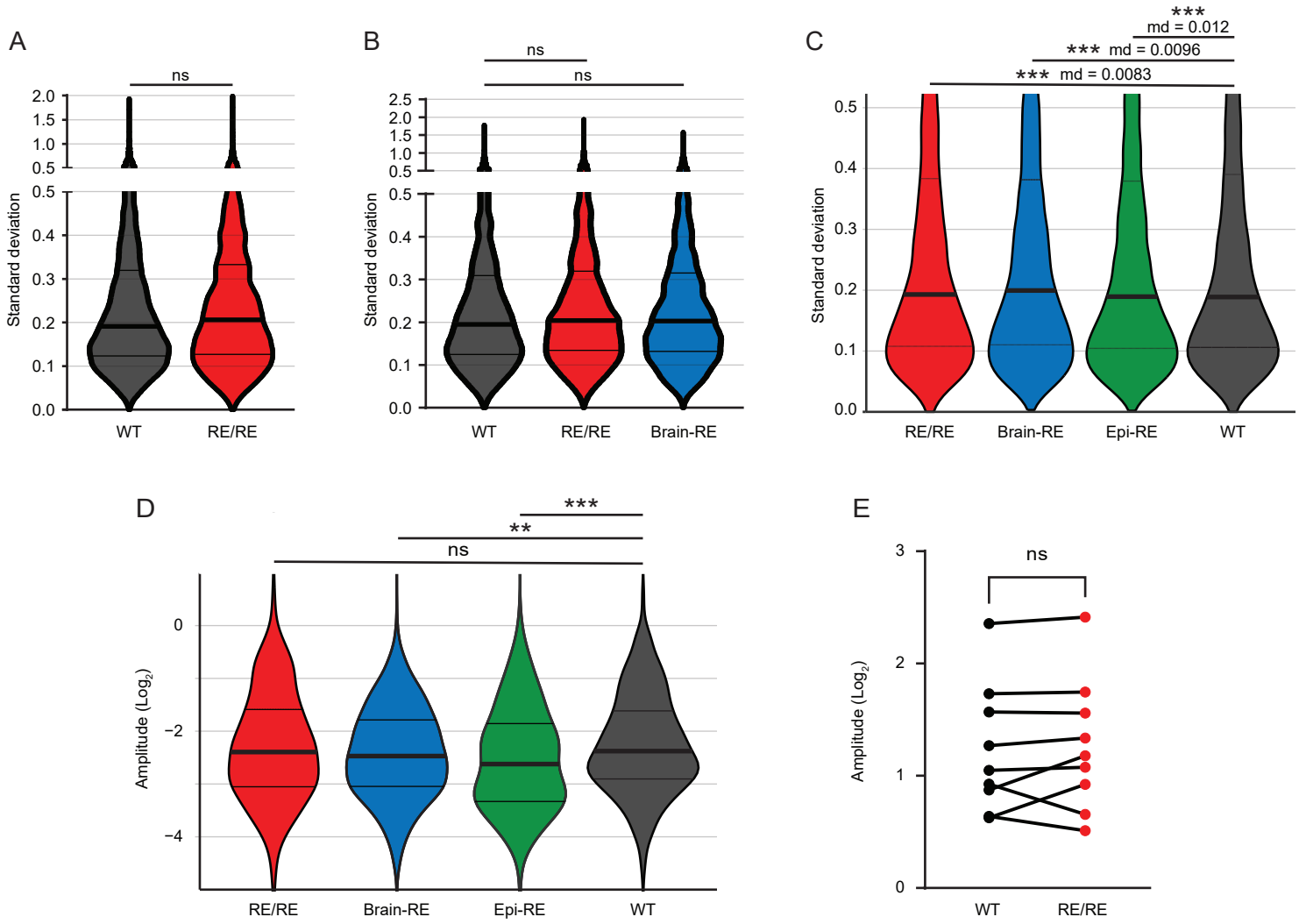

Supplementary Figure 3

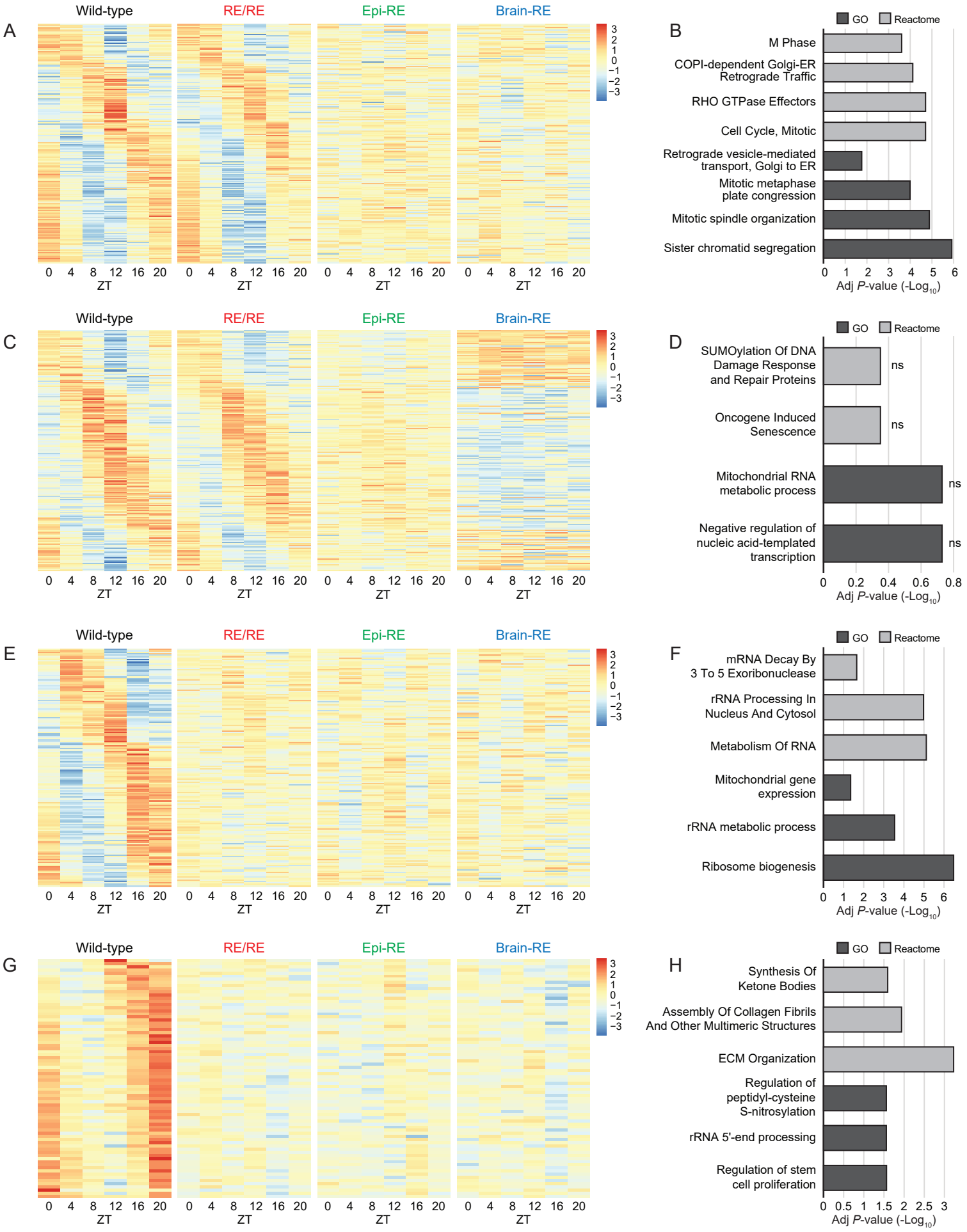

Supplementary Figure 4

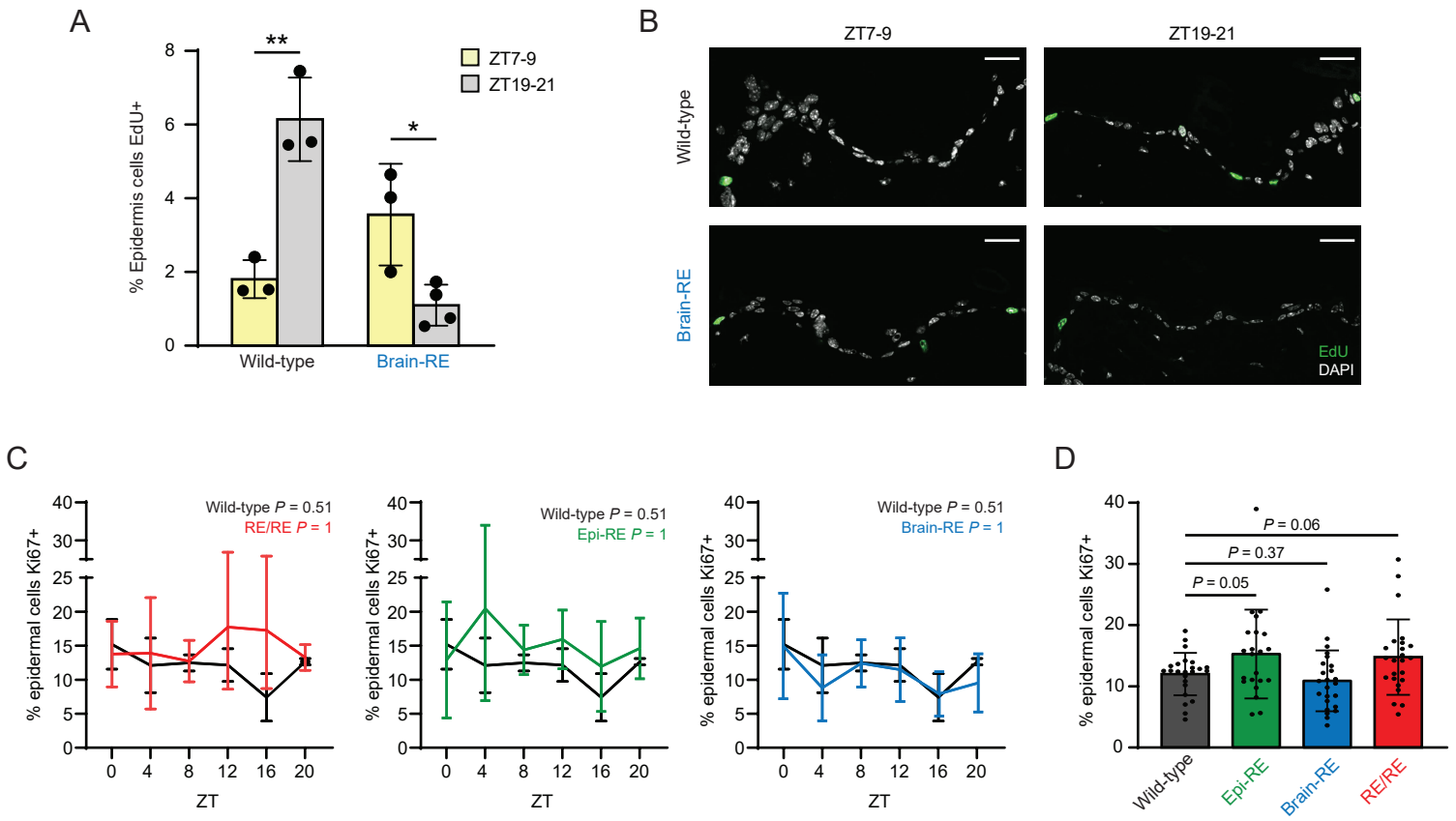

Supplementary Figure 5

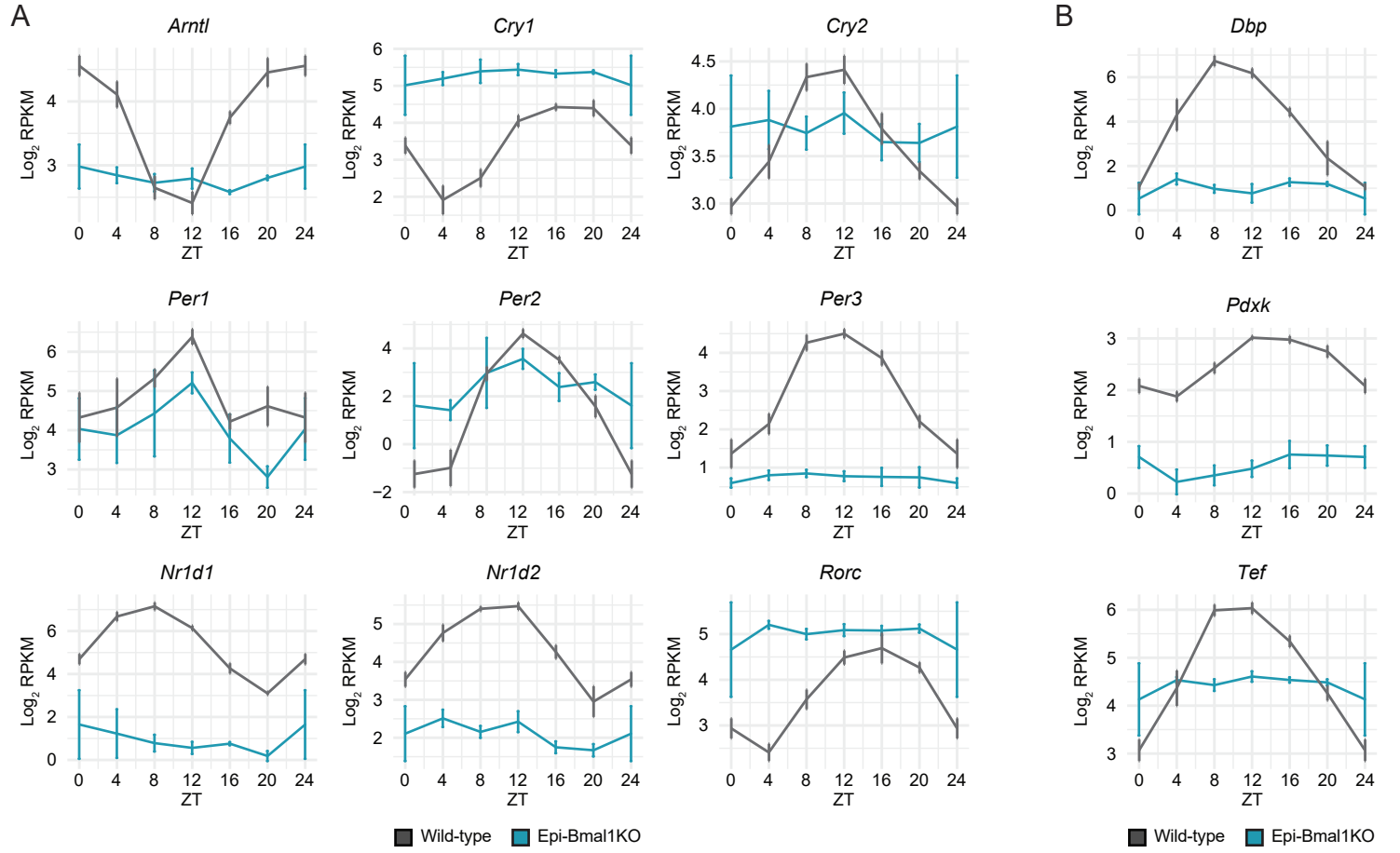

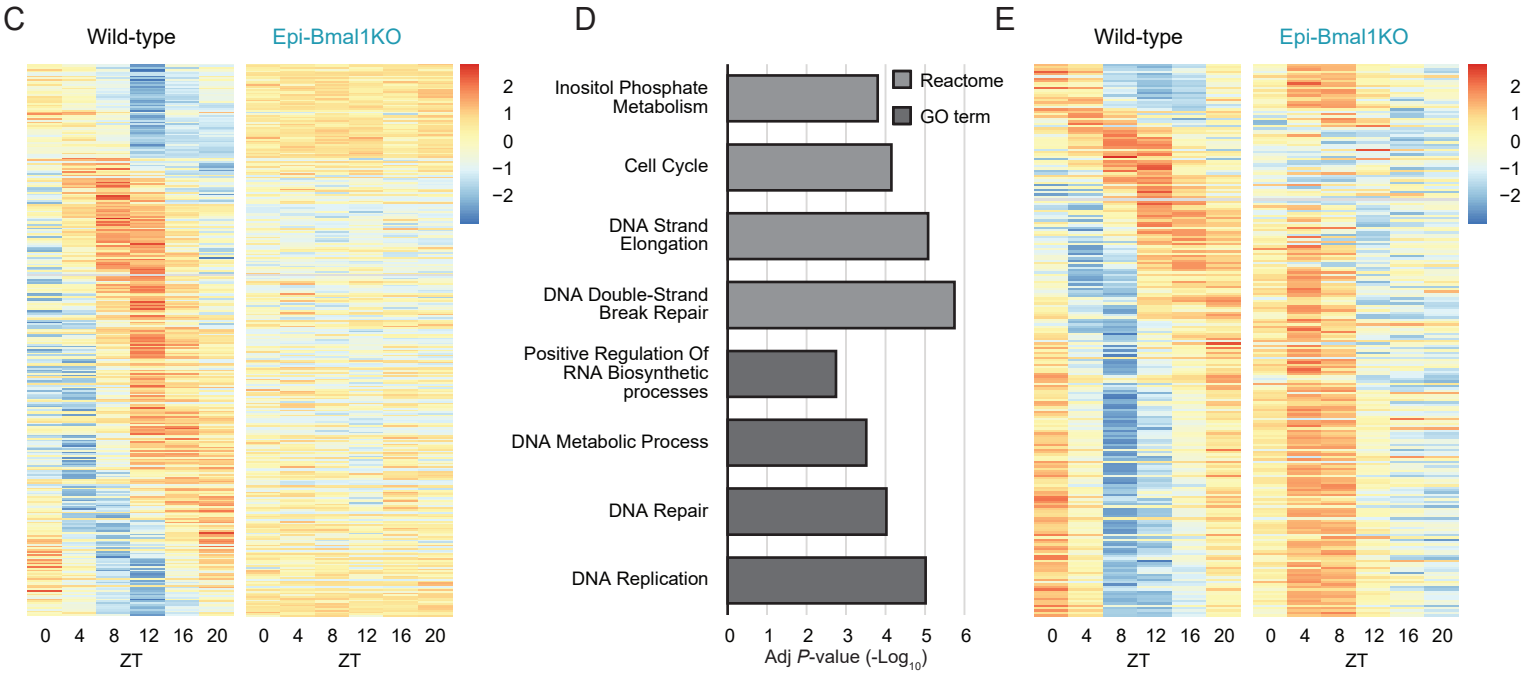

Supplementary Figure 6

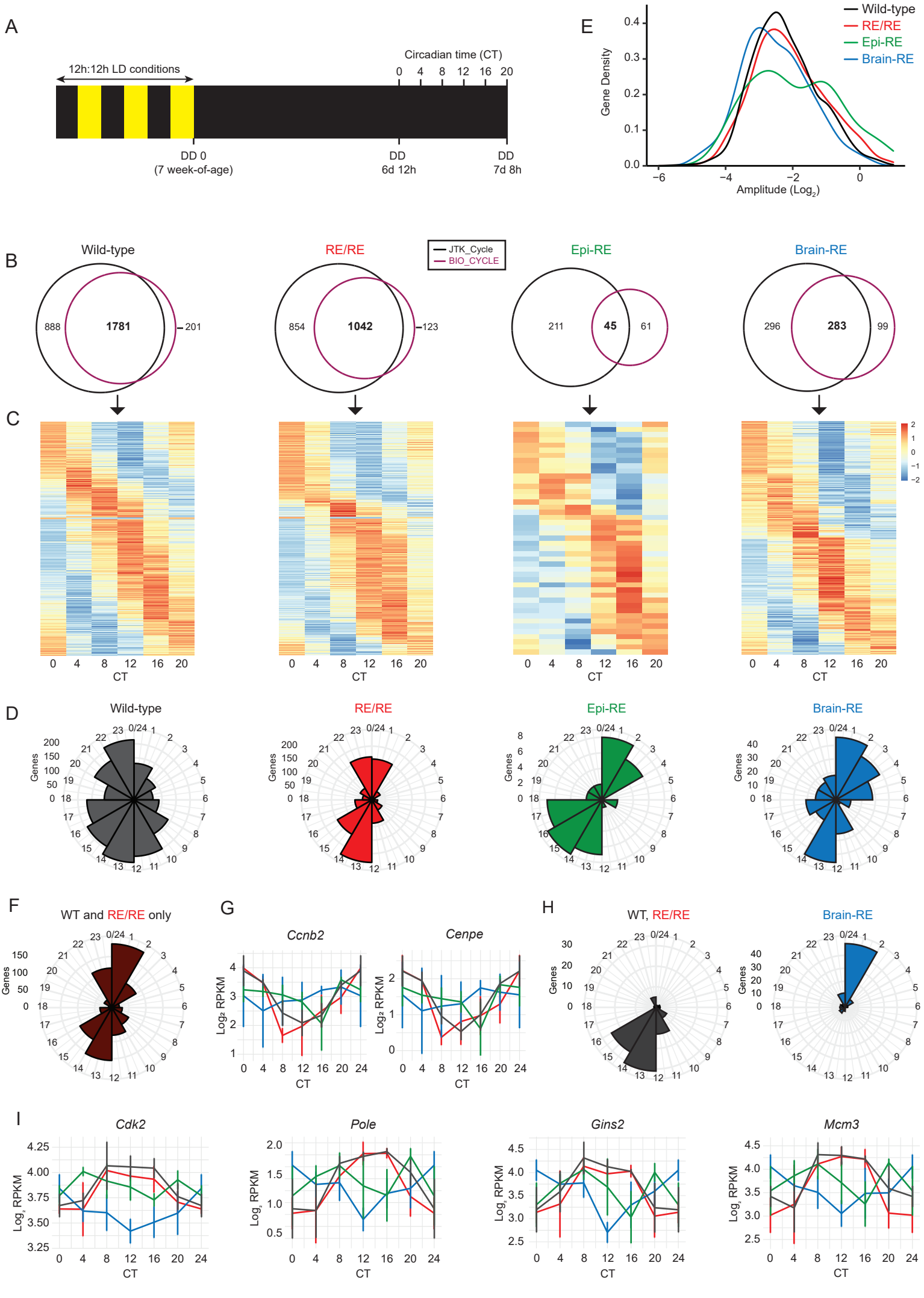

Click here to access/download

Supplemental Videos and Spreadsheets

Table S1.xlsx

Click here to access/download

Supplemental Videos and Spreadsheets

Table S2.xlsx

CELL PRESS DECLARATION OF INTERESTS POLICY

Transparency is essential for a reader's trust in the scientific process and for the credibility of published articles. At Cell Press, we feel that disclosure of competing interests is a critical aspect of transparency. Therefore, we require a "declaration of interests" section in which all authors disclose any financial or other interests related to the submitted work that (1) could affect or have the perception of affecting the author's objectivity or (2) could influence or have the perception of influencing the content of the article.

What types of articles does this apply to?

We require that you disclose competing interests for all submitted content by completing and submitting the form below. We also require that you include a "declaration of interests" section in the text of all articles even if there are no interests to declare.

What should I disclose?

We require that you and all authors disclose any personal financial interests (e.g., stocks or shares in companies with interests related to the submitted work or consulting fees from companies that could have interests related to the work), professional affiliations, advisory positions, board memberships (including membership on a journal's advisory board when publishing in that journal), or patent holdings that are related to the subject matter of the contribution. As a guideline, you need to declare an interest for (1) any affiliation associated with a payment or financial benefit exceeding $10,000 p.a. or 5% ownership of a company or (2) research funding by a company with related interests. You do not need to disclose diversified mutual funds, 401ks, or investment trusts.

Authors should also disclose relevant financial interests of immediate family members. Cell Press uses the Public Health Service definition of "immediate family member," which includes spouse and dependent children.

Where do I declare competing interests?

Competing interests should be disclosed on this form as well as in a "declaration of interests" section in the manuscript. This section should include financial or other competing interests as well as affiliations that are not included in the author list. Examples of "declaration of interests" language include:

> "AUTHOR is an employee and shareholder of COMPANY."
> "AUTHOR is a founder of COMPANY and a member of its scientific advisory board."

NOTE: Primary affiliations should be included with the author list and do not need to be included in the "declaration of interests" section. Funding sources should be included in the "acknowledgments" section and also do not need to be included in the "declaration of interests" section. (A small number of front-matter article types do not include an "acknowledgments" section. For these articles, reporting of funding sources is not required.)

What if there are no competing interests to declare?

If you have no competing interests to declare, please note that in the "declaration of interests" section with the following wording:

> "The authors declare no competing interests."

CELL PRESS DECLARATION OF INTERESTS FORM

If submitting materials via Editorial Manager, please complete this form and upload with your initial submission. Otherwise, please email as an attachment to the editor handling your manuscript.

Please complete each section of the form and insert any necessary "declaration of interests" statement in the text box at the end of the form. A matching statement should be included in a "declaration of interests" section in the manuscript.

Institutional affiliations

We require that you list the current institutional affiliations of all authors, including academic, corporate, and industrial, on the title page of the manuscript. ***Please select one of the following:***

☐ All affiliations are listed on the title page of the manuscript.

☒ I or other authors have additional affiliations that we have noted in the "declaration of interests" section of the manuscript and on this form below.

Funding sources

We require that you disclose all funding sources for the research described in this work. ***Please confirm the following:***

☒ All funding sources for this study are listed in the "acknowledgments" section of the manuscript.*

*A small number of front-matter article types do not include an "acknowledgments" section. For these, reporting funding sources is not required.

Competing financial interests

We require that authors disclose any financial interests and any such interests of immediate family members, including financial holdings, professional affiliations, advisory positions, board memberships, receipt of consulting fees, etc., that:

(1) could affect or have the perception of affecting the author's objectivity, *or*
(2) could influence or have the perception of influencing the content of the article.

Please select one of the following:

☒ We, the authors and our immediate family members, have no financial interests to declare.

☐ We, the authors, have noted any financial interests in the "declaration of interests" section of the manuscript and on this form below, and we have noted interests of our immediate family members.

Advisory/management and consulting positions

We require that authors disclose any position, be it a member of a board or advisory committee or a paid consultant, that they have been involved with that is related to this study. We also require that members of our journal advisory boards disclose their position when publishing in that journal. ***Please select one of the following:***

☒ We, the authors and our immediate family members, have no positions to declare and are not members of the journal's advisory board.

☐ The authors and/or their immediate family members have management/advisory or consulting relationships noted in the "declaration of interests" section of the manuscript and on this form below.

Patents

We require that you disclose any patents related to this work by any of the authors or their institutions. ***Please select one of the following:***

☒ We, the authors and our immediate family members, have no related patents to declare.

☐ We, the authors, have a patent related to this work, which is noted in the "declaration of interests" section of the manuscript and on this form below, and we have noted the patents of immediate family members.

Please insert any "declaration of interests" statements in this space. This exact text should also be included in the "declaration of interests" section of the manuscript. If no authors have a competing interest, please insert the text, "The authors declare no competing interests."

SAB is a co-founder and scientific advisor of ONA Therapeutics. PMC is an employee of Altos Laboratories.

☒ **On behalf of all authors, I declare that I have disclosed all competing interests related to this work. If any exist, they have been included in the "declaration of interests" section of the manuscript.**